nature communications

Article

https://doi.org/10.1038/s41467-024-51187-y

Full-scale polymer relaxation induced by single-chain confinement enhances mechanical stability of nanocomposites

Received: 10 January 2024

Accepted: 31 July 2024

Published online: 08 August 2024

Check for updates

Jin Huang[1], Hangsheng Zhou[1,2], Longhao Zhang[1], Li Zhang[1], Wei Shi[1], Yingchao Yang[1], Jiajia Zhou[3], Tianyi Zhao[1] & Mingjie Liu[1,4]

Polymer nanocomposites with tuning functions are exciting candidates for various applications, and most current research has focused on static mechanical reinforcement. Actually, under service conditions of complex dynamic interference, stable dynamic mechanical properties with high energy dissipation become more critical. However, nanocomposites often exhibit a trade-off between static and dynamic mechanics, because of their contradictory underlying physics between chain crosslinking and chain relaxation. Here, we report a general strategy for constructing ultra-stable dynamic mechanical complex fluid nanocomposites with high energy dissipation by infusing complex fluids into the nanoconfined space. The key is to tailor full-scale polymer dynamics across an exceptionally broad timescale by single-chain confinement. These materials exhibit stable storage modulus (10^0 ~ 10^2 MPa) with high energy dissipation (loss factor > 0.4) over a broad frequency range (10^{-1} ~ 10^7 Hz)/temperature range (−35 ~ 85°C). In the loss factor > 0.4 region, their dynamic mechanical stability (rate of modulus change versus temperature (k)) is 10 times higher than that of conventional polymer nanocomposites.

Polymer nanocomposites with unique ability to tune specific mechanical, electrical, thermal, and optical properties are exciting candidates for a variety of current and future technologies[1–3]. In recent decades, most research has focused on the static mechanical reinforcement of polymer nanocomposites, especially strength and toughness[4,5]. Mechanical reinforcement is essentially the tuning of the interphase formed by interfacial polymer layer bound to nanofiller surfaces, which can interact with and modify the polymer matrix[5–8]. Many empirical strategies of tuning interphase have been developed, including processing techniques[9–11], chain structure[12–14], nanofiller-polymer interaction[15–17], and nanofiller arrangement[18–20]. These strategies severely restricting polymer chain relaxation inevitably sacrifice energy dissipation of polymer nanocomposites due to dense covalent/noncovalent cross-links and supramolecular interactions induced by the introduction of attractive nanofillers[21,22]. Moreover, a precipitous drop in the modulus of several decades is unavoidable in a small temperature/frequency variation, due to the dissociation of supramolecular interactions and the glass transition[23]. In fact, polymer nanocomposites constantly face complex dynamic mechanical interference (such as periodic vibration and stress shock) and wide temperature variations during service, where stable dynamic mechanics with high energy dissipation becomes more critical. However, nanocomposites often exhibit a trade-off between static and dynamic mechanics, because of their

[1]Key Laboratory of Bioinspired Smart Interfacial Science and Technology of Ministry of Education, School of Chemistry, Beihang University, Beijing 100191, P. R. China. [2]National Key Lab of Spintronics, Hangzhou International Innovation Institute, Beihang University, Hangzhou 311115, P. R. China. [3]South China Advanced Institute for Soft Matter Science and Technology, School of Molecular Science and Engineering, South China University of Technology, Guangzhou 510640, P. R. China. [4]Center for Bioinspired Science and Technology, Hangzhou International Innovation Institute, Beihang University, Hangzhou 311115, P. R. China. e-mail: liumj@buaa.edu.cn

contradictory underlying physics between chain crosslinking and chain relaxation.

Herein, we report stable dynamic mechanical complex-fluid gels (CFGs) with high energy dissipation over a broad frequency range by infusing complex fluids (polymer fluids and nanoparticles) into the multicomponent networks. The key is to tailor the full-scale polymer dynamics across an exceptionally broad timescale through the method of single-chain confinement, resolving the concentrated chain relaxation distribution of polymer materials. Moreover, matrix chains dynamically couple with adsorbed chains on the nanofiller interphase, providing an effective non-crosslinking stiffening mechanism for polymeric materials. CFGs combine high-performance dynamic and static mechanics with elastic modulus on the order of megapascals. They exhibit stable storage modulus (G') of 10^0 ~ 10^2 MPa and loss factor (tanδ) of 0.4 ~ 0.8 over a broad frequency range (10^{-1} ~ 10^7 Hz) and temperature range of −35 ~ 85°C, where the variations of tanδ and G' are extremely steady and their amplitudes are low. Their dynamic mechanical stability far exceeds that of typical state-of-the-art polymer nanocomposites. In acoustic absorption experiments, sound absorption coefficient of the CFG (larger than 0.3) is over 2 times higher than that of commercial damping materials in each frequency band, and its curve displays a stable trend. CFGs are of significance to extend the availability of polymer nanocomposites in the practical applications for complex operating environments.

Results

Traditional polymer nanocomposites are characterized by strong friction of short-range segmental relaxation and free oscillation of several segments (Fig. 1). Segmental relaxation is accompanied by a precipitous decrease in the modulus of several orders of magnitude in a narrow frequency range, leading to dynamic mechanical instability. Therefore, to obtain stable dynamic mechanical polymer nanocomposites with high energy dissipation, we need to significantly broaden the relaxation time distribution of polymer chains in the system, achieved by tailoring full-scale polymer dynamics through the method of single-chain confinement (Fig. 1a(ii)). The relaxation modes can be mainly divided into segmental dynamics, Rouse dynamics and chain diffusion according to the length scale (Fig. 1b(ii)). Segmental dynamics is dominated by the dynamic heterogeneity of cooperative regions, where cooperative regions take 2–4 nm transient molecular clusters reorienting distinct configurations[24,25]. Segmental dynamics near the nanoparticle surface is heterogenous. Their relaxation time decreases smoothly from the solid surface into the matrix. The surface-to-surface distance (d) of nanoparticles is small enough that the interfacial zones overlap, broadening their relaxation time distribution. Rouse dynamics, also called intermediate dynamics, is the collective motion of several chain segments[26]. Polymer chains adsorbed atop a solid surface can form multiple conformations (tails, loops and trains)[27] with different activated energy barriers of Rouse dynamics, leading to hierarchical relaxations of several chain segments. Due to the presence of nanoparticles, the chain diffusion is geometrically confined and subjected to viscous drag force, where the chains exhibit sticky reptation[28]. In this case, the particle obstacle hinders chain diffusion, different from the standard chain entanglements occurring in the flow state. Moreover, in the nanoconfined space of the chain size, all matrix chains dynamically couple with adsorbed chains on nanofiller interphase, providing an effective non-crosslinking stiffening mechanism for polymeric materials. This can further improve the dynamic mechanical stability of polymer nanocomposites, while also ensuring their high static mechanics.

To validate the above proposed concept, these synthesized polymer nanocomposites should contain linear polymer fluids, nanofillers and multicomponent networks. We selected three polymers with extremely different glass transition temperatures (T_g) of poly(stearyl methacrylate) (PSMA), poly(lauryl methacrylate) (PLMA) and poly(tert-butyl acrylate) (PtBA) for random copolymerization to form a homogeneous copolymer network, regulating segmental dynamic heterogeneity in the system[29] (Supplementary Fig. 1). Meanwhile, these polymers contain long side chains, which provide strong internal friction of chain segment relaxation. The polymer fluid is formed by flexible PLMA with a low T_g (−65 °C). By adjusting the chain length through the molecular weights of PLMA ($M_{n\ (\mathrm{PLMA\ fluid})}$), the polymer radius of gyration (R_g) of the polymer fluid can be precisely tailored, and their associated calculation is shown in Methods. The molecular characteristics of all synthesized PLMA fluids are provided in Supplementary Fig. 2 and Supplementary Table 1. The added nanofillers are hydrophobic silica (SiO_2) nanoparticles, because their aggregate state is better controlled than that of other dimensions of nanofillers. The specific preparation strategy of our complex-fluid-gels (CFGs) is shown in the Supplementary Information. The mechanical properties of CFGs are mainly controlled by the following structural parameters: weight fraction of PLMA fluid ($\Phi_{\mathrm{PLMA\ fluid}}$), molecular weight of PLMA fluids ($M_{n\ (\mathrm{PLMA\ fluid})}$), SiO_2 nanoparticle size, weight fraction of nanoparticles (Φ_{NP}), and weight fraction of network components (Φ_{Network}). The molecular characteristics of all synthesized materials are listed in Supplementary Tables 2, 3, 7 and 8.

We investigated the dynamic response properties of the CFGs with different molecular structures by employing an oscillatory strain rheometer, and constructed the dynamic master curves of CFGs by time-temperature superposition (TTS). We first analyzed the effect of chain length ($M_{n\ (\mathrm{PLMA\ fluid})}$) of the polymer fluid on the dynamic mechanical properties of CFGs. Without the polymer network, the rheological behavior of PLMA with various M_n was investigated at 25°C as shown in Supplementary Fig. 3. The low M_n PLMA fluids (M_n = 24k and 75k) display viscous flow behavior and lack the entanglement platform region, whose curves show the characteristics of unentangled polymer melts. In contrast, the higher $M_{n\ (\mathrm{PLMA\ fluid})}$ fluids ($M_{n\ (\mathrm{PLMA\ fluid})}$ larger than critical entanglement molecular weight (M_e = 144k)) exhibit entanglement plateau region[30]. Subsequently, we further investigated the viscoelastic behavior of the polymer fluid with nanoparticles in this system. Supplementary Fig. 4 shows the frequency dependence of master curves of storage modulus (G') and loss factor (tanδ) for PLMA fluids with $\Phi_{\mathrm{NP\text{-}14nm}}$ = 20% and varying $M_{n\ (\mathrm{PLMA\ fluid})}$. Due to the existence of nanoparticles, their G' is significantly improved, and their whole chain relaxation time is several orders of magnitude slower than that of pure PLMA fluid. As $M_{n\ (\mathrm{PLMA\ fluid})}$ increases to 165k (larger than M_e), the nanocomposite fluids do not exhibit viscous flow behavior in the low frequency region, but show gel-like characteristics. It arises from the dynamic percolating network formed between the entangled polymer chains and nanoparticles[31]. As $M_{n\ (\mathrm{PLMA\ fluid})}$ is further increased, their G' slightly increases and tanδ gradually decreases, because PLMA fluid is too entangled to relax.

In the CFGs, G' shows a similar trend to the nanocomposite fluids, increasing with the increase of $M_{n\ (\mathrm{PLMA\ fluid})}$ (Fig. 2a(i)). The situation is quite different for tanδ in the mid/low frequencies. When $M_{n\ (\mathrm{PLMA\ fluid})}$ is less than 165k (M_e), tanδ increases with the increase of $M_{n\ (\mathrm{PLMA\ fluid})}$ (Fig. 2a(ii)). The modulus (G' and loss modulus (G'')) of polymer fluids in the network are low, since chain length of polymer fluids is too short to be entangled and they are in the viscous flow state, as can be seen from Supplementary Fig. 4. In this case, their energy dissipation (tanδ) is low, like elastomers with crosslinked polymers. As $M_{n\ (\mathrm{PLMA\ fluid})}$ is larger than M_e, tanδ decreases with the increase of $M_{n\ (\mathrm{PLMA\ fluid})}$, for the same reason for nanocomposite fluids. To ensure optimal mechanical and damping properties of CFGs, we should regulate $M_{n\ (\mathrm{PLMA\ fluid})}$ of the added PLMA fluid slightly higher than its own M_e. To further understand these interactions, we performed amplitude sweeps of CFGs with varying $M_{n\ (\mathrm{PLMA\ fluid})}$. As shown in Supplementary Fig. 5, all CFGs do not show obvious modulus reduction (Payne effect) at small strain, indicating that there are no aggregations of nanoparticles in the PLMA matrix. With increasing strain, CFGs with high molecular weight

https://doi.org/10.1038/s41467-024-51187-y

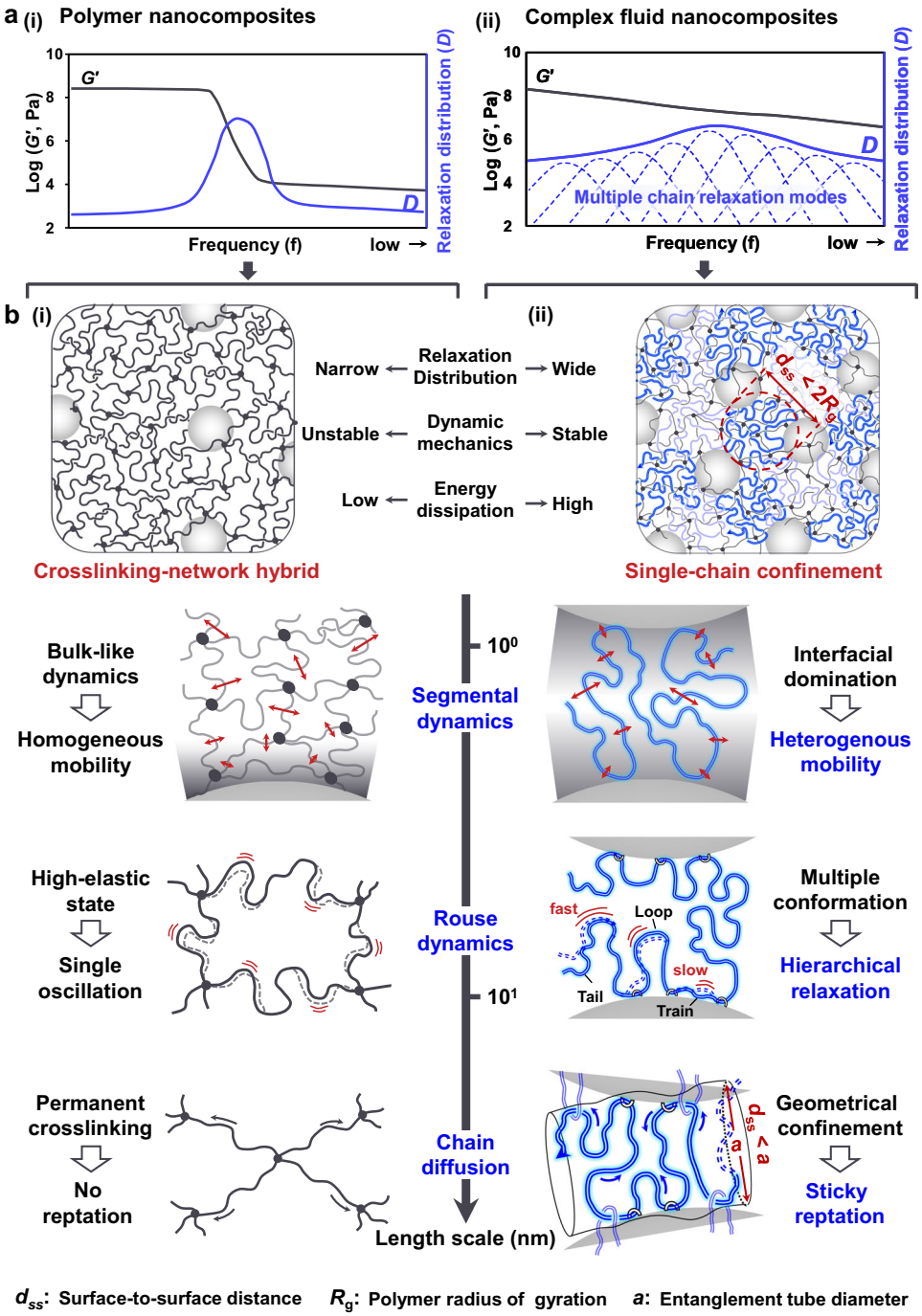

Fig. 1 | Design concept for ultra-stable dynamic mechanics in polymer nanocomposites. a Mechanical properties and chain relaxation time distribution of traditional polymer nanocomposites and complex fluid nanocomposites. **b** Strategies for tailoring full-scale polymer relaxation induced by single-chain confinement in polymer nanocomposites. (i) Traditional nanocomposites have only strong frictional short-range segmental dynamics and free oscillating Rouse dynamics. (ii) Full-scale regulation of polymer dynamics across an exceptionally broad timescale can be achieved by the method of single-chain confinement in complex fluid nanocomposites. In this case, we regulate the chain dynamics at different length scales, divided into the segmental dynamics, Rouse dynamics and chain diffusion. The relaxation time of segmental dynamics decreases smoothly from the solid surface into the matrix, exhibiting heterogenous dynamics. The surface-to-surface distance (d_{ss}) of nanoparticles is so small that interfacial zones overlap. Rouse dynamics is the collective motion of several chain segments. Polymer chains adsorbed atop a solid surface can form multiple conformations (tails, loops and trains) with different activated energy barriers of Rouse dynamics, leading to hierarchical relaxations of several chain segments. Due to the existence of nanoparticle obstacles, the chain diffusion is geometrically confined, where chains are subjected to viscous drag force and their sticky reptation occurs.

exhibit a more pronounced Payne effect. It arises from the breakup of the bridging effects between the nanofiller surface and polymer chains (Supplementary Fig. 5b). In addition, CFGs containing high M_n PLMA show a more pronounced reduction in modulus after 100% cyclic strain (Supplementary Fig. 5a and c). This suggests that there are damaged physical interactions or topological structures that cannot be restored in the short term.

We then investigated how the surface-to-surface distance of nanoparticles (d_{ss}) affects the dynamic mechanical properties of CFGs. The d_{ss} is controlled by two structural parameters: size and

https://doi.org/10.1038/s41467-024-51187-y

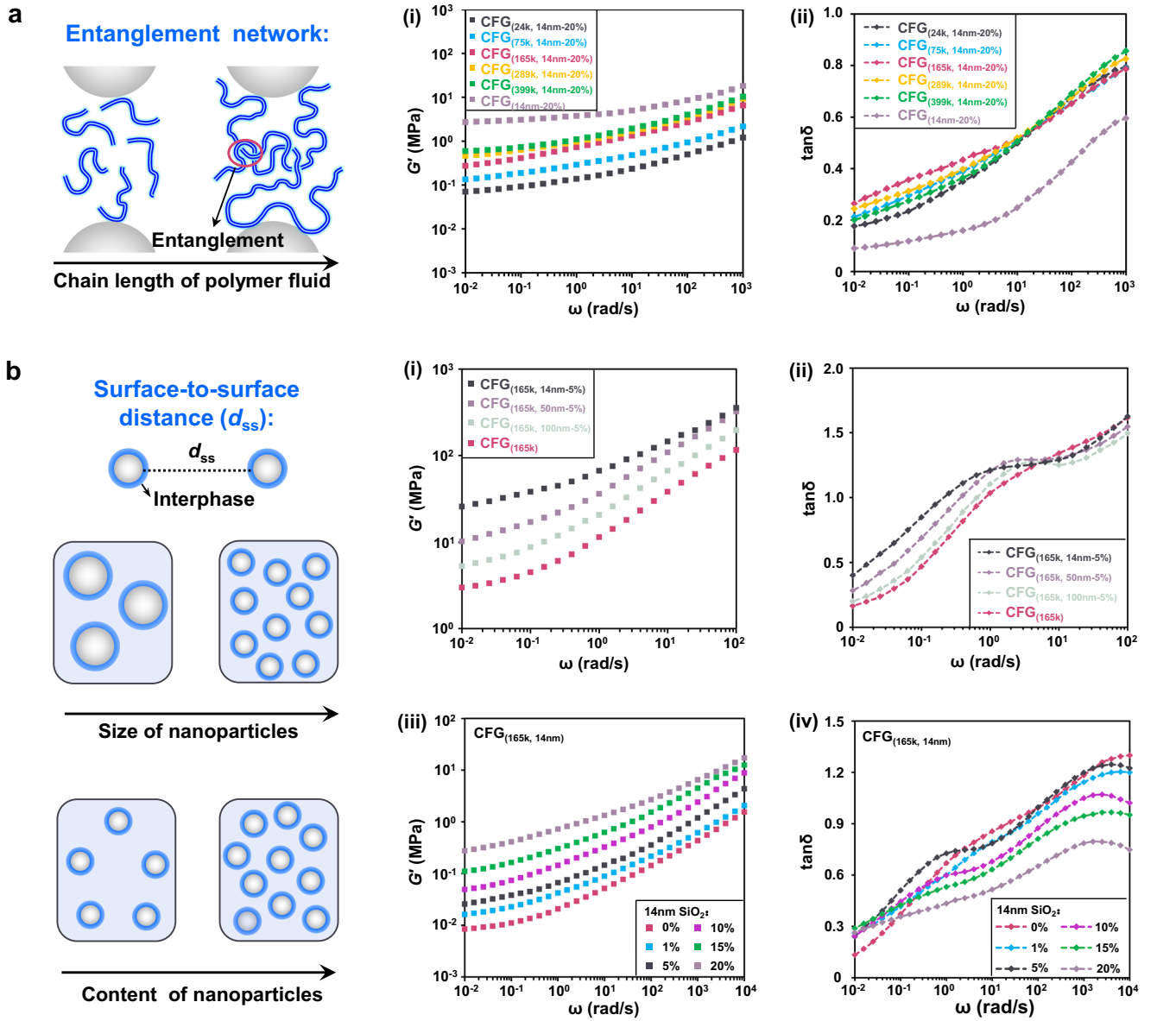

Fig. 2 | Rheological behaviour of complex-fluid-gels (CFGs). a Frequency dependence of master curves of storage modulus (G') and loss factor (tanδ) for CFGs with $\Phi_{nanoparticle}$ = 20% and varying $M_{n\ (PLMA\ fluid)}$. **b** (i and ii) Frequency dependence of master curves of G' and tanδ for CFGs with $\Phi_{nanoparticle}$ = 5% and varying particle sizes. (iii and iv) Frequency dependence of master curves of G' and tanδ for CFGs with varying $\Phi_{nanoparticle}$ of 14 nm nanoparticles. In the CFGs, changing the content and size of particles is essentially to regulate the surface-to-surface distance of particles (d_{ss}). In all CFGs, master curves were prepared by the time-temperature superposition treatment at 25°C with a constant shear strain of 0.5%, and the weight ratio of crosslinker / PLMA monomer / PLMA fluid is 3:100:150. $M_{n\ (PLMA\ fluid)}$: molecular weight of PLMA fluids, $\Phi_{nanoparticle}$: weight fraction of nanoparticle, $\Phi_{PLMA\ fluid}$: weight fraction of PLMA fluid.

content of nanoparticles. Master curves of CFGs with different particle sizes are shown in Fig. 2a(i) and (ii). The storage modulus (G') and loss factor (tanδ) increase as the particle size decreases. The reason is that the d_{ss} of nanoparticles decreases as their size decreases, significantly improving the dynamic coupling between the interphase of nanoparticles and the polymer matrix. This can be confirmed by the fact that the whole chain relaxation of the PLMA fluid with Φ_{NP} = 5% slows down as the particle size decreases (Supplementary Fig. 6). In addition, we further investigated the effect of d_{ss} on the mechanical properties of CFGs by controlling particle content (Φ_{NP}) (Fig. 2b(iii) and (iv)). G' increases with increasing the content of particles, while the peak value of tanδ becomes smaller and its changing trend displays more stable. Without the polymer network, the value of tanδ curve of the polymer fluid with high particle content (Φ_{NP} = 20%) remains about 0.5 at frequencies from 10^{-2} to 10^{2} rad/s (Supplementary Fig. 7), which shows frequency-insensitive energy dissipation property. As a consequence, we can achieve dynamic mechanical stability with high energy dissipation in CFGs by controlling the aggregation of complex fluids.

To analyze such an enhancement mechanism of dynamic mechanical stability in CFGs, we investigated the law of chain relaxation with the particle aggregation. Figure 3a shows SAXS results of the CFGs with different contents of 14 nm nanoparticles. The curve of the CFG with low nanoparticle loading ($\Phi_{14nm\text{-}NP}$ = 1%) shows good agreement with a single NP form factor, obtained from the dilute solution of well-dispersed nanoparticles (2 mg/mL in toluene). These data show that the nanoparticles are well dispersed in the PLMA matrix. All scattering curves of nanoparticle systems with different loading show a plateau in the low wave vector (q) region, which is a signature of essentially uniform distribution of

https://doi.org/10.1038/s41467-024-51187-y

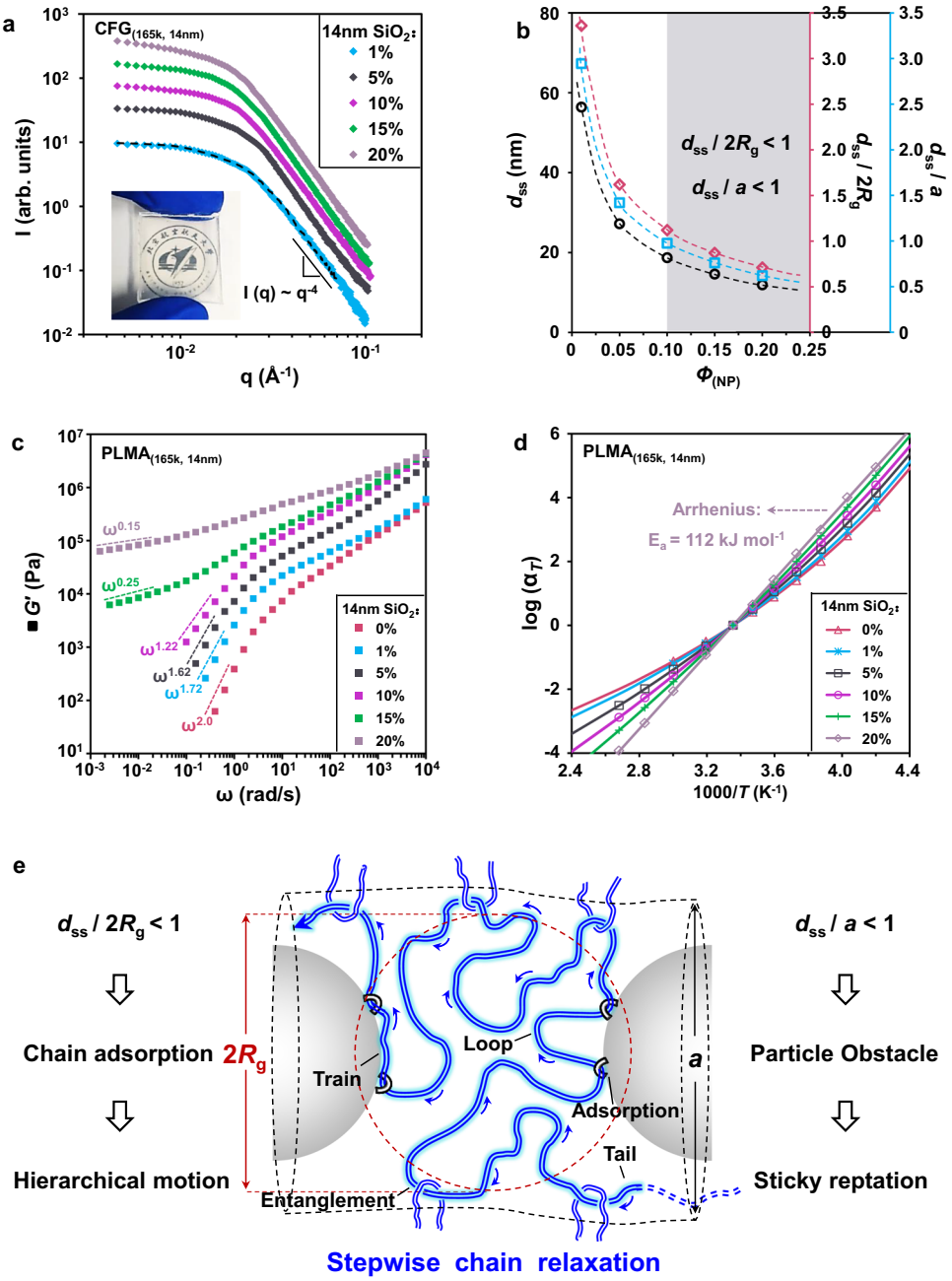

Fig. 3 | Stepwise chain relaxation of complex fluid in the CFGs. a SAXS results of the CFGs with varying content of 14 nm nanoparticles. The SAXS shows well-dispersed nanoparticle systems at the different loadings, as manifested by a low-q plateau. Moreover, the slopes in the Porod region are all −4, further confirming the individual nanoparticle dispersion with sharp interfaces. **b** The surface-to-surface distance (d_{ss}), d_{ss} / $2R_g$ (polymer radius of gyration) and d_{ss} / a (entanglement tube diameter) as a function of weight fraction of nanoparticles (Φ_{NP}) in the CFGs. As Φ_{NP} exceeds 10% (gray region), d_{ss} is smaller than the entanglement tube diameter and the chain size ($2R_g$), indicating that the polymer chains are geometrically constrained. **c** Frequency dependence of storage modulus (G') of PLMA fluids with increasing Φ_{NP}. In the low frequency region, G' increases as an approximate power law function, $G'(\omega) \sim \omega^{\alpha}$. When Φ_{NP} is larger than 10%, the power-law exponent α obviously less than 2. **d** Temperature dependence of the shift factor (α_T) of PLMA with varying nanoparticle loading. The solid lines are fitted by WLF equation, where 20% data simultaneously is ideally matched with Arrhenius equation. Fitting parameters are listed in Supplementary Table 6. **e** The illustration of stepwise chain relaxation mechanism for CFGs.

nanoparticles. In this low-q region, we plotted ln(I) as a function of q^2 (Supplementary Fig. 8). This curve is linear, an indication of the uniformity of size, and its slope is equal to −16.58 nm^2. Since its slope is $-R_{g(NP)}^2/3$ ($R_{g(NP)}$, nanoparticle radius of gyration), $2R_{g(NP)}$ can be calculated to be 14.2 nm, in agreement with the values reported by the supplier[32]. Moreover, the Porod region slopes are all approximately equal to −4, further confirming the individual nanoparticle dispersion with sharp interfaces[33]. The inset for the photograph of CFG with $\Phi_{14nm\text{-}NP}$ = 20% shows excellent transparency, also indicating the good dispersion of nanoparticles to some extent.

Based on these characterization results of nanoparticle dispersion in the polymer matrix, the surface-to-surface distance of nanoparticles (d_{ss}) can be calculated by the random distribution of spheres. The specific calculation is $2R_{NP}[(2 / \pi\Phi_{NP})^{1/3} - 1]$, where R_{NP} is the radius of the nanoparticle[7]. To analyze the effect of the nanoparticle confinement on chain relaxation, we calculated d_{ss} / $2R_g$ (polymer radius of gyration)

and d_{ss} / a (entanglement tube diameter) of CFGs with varying $\Phi_{14nm\text{-}NP}$ (Fig. 3b and Supplementary Table 4), where a was calculated in Methods. When Φ_{NP} exceeds 10% (gray region in Fig. 3b), d_{ss} is smaller than the entanglement tube diameter and the chain size ($2R_g$), indicating that the polymer chains are geometrically constrained.

We systematically compared the polymer chain dynamics of nanocomposite PLMA fluids with varying $\Phi_{14nm\text{-}NP}$. As the temperature dependent heat capacity (C_p) of nanocomposite PLMA fluids shown in the Supplementary Fig. 9, the glass transition exhibits a noticeable broadening when $\Phi_{14nm\text{-}NP}$ increases, while the overall strength of this transition is not affected significantly. This can be inferred that the segmental relaxation of polymer chains adsorbed onto the nanofiller interface is not fully suppressed, while presents an obvious broadening of the relaxation time distribution[34]. Figure 3c shows the frequency dependence of their storage modulus (G'). In the low frequency region, G' increases as an approximate power law function, $G'(\omega) \sim \omega^{\alpha}$, where the power-law exponent α equal to 2 is a characteristic of the whole chain relaxation of pure polymers ($\Phi_{14nm\text{-}NP} = 0$). This α is strongly dependent on the nanoparticle concentration. As $\Phi_{14nm\text{-}NP}$ increases to 20%, the α decreases from 2 to 0.15, indicating that the frequency dependence of G' becomes quite small and the neat liquid-like PLMA gradually transforms into a gel-like composite fluid[7]. In addition, the α (α = 0.15) of PLMA with $\Phi_{14nm\text{-}NP} = 20\%$ is almost unchanged over a broad frequency range (about $10^4 \sim 10^{-2}$ rad/s), reflecting that polymer chains exhibit a considerably wide distribution of short range chain relaxation.

To understand this transition of chain relaxation, we summarized the essential information on the temperature dependence of chain dynamics of complex fluids in Fig. 3d, Supplementary Fig. 10 and Supplementary Table 5, where the frequency shift factor (α_T) of PLMA with varying nanoparticle loading is plotted against the inverse temperature with $T_{ref} = 298$ K. The solid lines are fitted by the WLF equation, and their fitting parameters are listed in Supplementary Table 6. More interestingly, the data of PLMA with $\Phi_{14nm\text{-}NP} = 20\%$ simultaneously is ideally matched with Arrhenius behavior with activation energy $E_a = 112$ kJ/mol, reflecting that interchain interactions become less important in the global dynamics[35]. These facts can be explained that the interfacial adsorbed chains are indeed highly mobile internally with no glassy nature while their center-of-mass diffusion and some Rouse modes are suppressed due to adsorption.

Based on our results, we proposed the stepwise chain relaxation mechanism of CFGs to enhance the dynamic mechanical stability (shown in Fig. 3e). There are several relevant length scales to consider, namely, surface-to-surface distance of nanoparticles (d_{ss}), polymer chain size ($2R_g$), and entanglement tube diameter (a). At $\Phi_{14nm\text{-}NP} = 20\%$ where d_{ss} is significantly less than $2R_g$, all polymer chains are adsorbed atop nanoparticles, forming multiple conformations (tails, loops, and trains) with different entropic barriers of Rouse dynamics for polymer chains. This can lead to hierarchical relaxations of several chain segments. Under these circumstances, the d_{ss} is also less than a. Due to the existence of particle obstacle, the chain diffusion is subjected to viscous drag force, where sticky reptation of chains will occur. Hence, we have realized the design concept for the regulation of stepwise chain relaxation with multiple length scales proposed in Fig. 1. Moreover, in the absence of the "free" chains at high Φ_{NP}, all matrix chains dynamically couple with adsorbed chains on nanofiller interphase, providing an effective non-crosslinking stiffening mechanism. This endows polymer nanocomposites with high static mechanics, resulting in the improvement of their dynamic mechanical stability.

To maximize the dynamic mechanical stability and energy dissipation performance of CFGs, we also need to regulate segmental dynamics of polymer chains, arrived at via adjusting polymer component heterogeneity (Fig. 4a). Specifically, the solution is to design a multicomponent network by random copolymerization of multiple polymers with extremely different glass transition temperatures (T_g), namely, poly(stearyl methacrylate) (PSMA, T_g = -100°C), poly(lauryl methacrylate) (PLMA, T_g = -65°C), and poly(tert-butyl acrylate) (PtBA, T_g = 44°C). Furthermore, these polymers contain long side chains that provide strong internal friction of chain segment relaxation. As a proof of principle, we prepared a series of CFGs by adjusting the proportion of polymer components, as shown in Supplementary Tables 7 and 8. First, we had to consider the phase separation behavior of polymer components, leading to mechanical instability of CFGs. Figure 4b and Supplementary Figs. 11 and 12 show AFM images of CFGs with different proportions of network components. As the PSMA content ($\Phi_{PSMA} = 10\%$) of the CFG ($CFG_{(2L,\ 4t,\ 2S,\ 0\%NP)}$) is 10%, there is no phase separation behavior in this system (Fig. 4b). The area of white bright domain gradually increases with the increase of PSMA content, indicating that the degree of crystallization in CFGs increases. To confirm that the white bright domain is formed by PSMA crystallization, we used the PeakForce QNM model of AFM to characterize the property that the crystallization melting will be accompanied by a sharp change in the modulus. Supplementary Fig. 13 shows the modulus versus temperature of bright domain in the CFG's AFM phase image (Fig. 4b). The modulus decreases sharply in the temperature range of 22 ~ 35°C, basically consistent with the reported crystallization melting temperature of PSMA.

In addition, we employed the rheometer and differential scanning calorimetry (DSC) to investigate the phase separation behavior of CFGs with multicomponent network. The temperature dependence of master curves of G', G'' and tanδ for $CFG_{(2L,\ 4t,\ 2S)}$ shows a fairly stable trend (Fig. 4c(i) and (ii)), and there is no crystallization melting peak in its DSC curve (Fig. 4c(iii)). With the further increase of Φ_{PSMA}, their dynamic master curves show a pronounced peak (Fig. 4c(i) and (ii)), due to the abrupt change of viscoelastic behavior caused by the melting of PSMA crystalline phase in CFGs. In this case, their DSC curves show crystallization melting peaks (Fig. 4c(iii)), where the peak value increases with the increase of Φ_{PSMA} and the peak position shifts to higher temperatures, indicating the increase of crystallinity in the system. These results validate that we can adjust the proportion of network components to interfere with PSMA crystallization behavior, and obtain a multicomponent network with a homogeneous phase, ensuring dynamic mechanical stability of CFGs.

We systematically studied the effect of network components on energy dissipation and mechanical properties of CFGs. When the mass ratio of PSMA, PLMA, and PtBA in the network of CFGs is 1:2:1, the $CFG_{(2L,\ 4t,\ 2S)}$ exhibits the widest frequency range of high energy dissipation (tanδ > 0.4) and the most stable mechanical properties, that is, the modulus change is the smallest in the range of tanδ > 0.4 (Supplementary Fig. 14). Its temperature-dependence master curves also show the same trend (Supplementary Fig. 15). Specifically, $CFG_{(2L,\ 4t,\ 2S)}$ exhibits considerably high tanδ (0.4 ~ 0.8) and G' ($10^0 \sim 10^2$ MPa) in the frequency range of $10^{-1} \sim 10^7$ Hz/temperature range of -35 ~ 85°C (Fig. 5a). The variation values of tanδ and G' are only within 0.4 and two orders of magnitude, respectively. Notably, its G' change rate (k) and tanδ change (Δ tanδ) in the temperature region of tanδ > 0.4 are far less than that of reported nanocomposites as shown in Fig. 5b and c and Supplementary Table 9. Their dynamic mechanical stability (rate of modulus change versus temperature (k)) is 10 times higher than that of conventional polymer materials, indicating that the CFG exhibits ultrahigh dynamic mechanical stability and energy dissipation over a broad frequency range. To visualize these properties of the CFG, acoustic absorption tests were conducted (Fig. 5d). The CFG can effectively attenuate sound waves over a broad frequency range. The sound absorption coefficient of the CFG (larger than 0.3) is significantly higher than that of commercial damping materials under any frequency band, and its curve displays a stable trend (Fig. 5e). In the electric motor vibration absorption demonstrative experiment, the CFG can effectively absorb vibration in all frequency bands, significantly better than commercial damping materials (Supplementary Fig. 16). In addition, the

https://doi.org/10.1038/s41467-024-51187-y

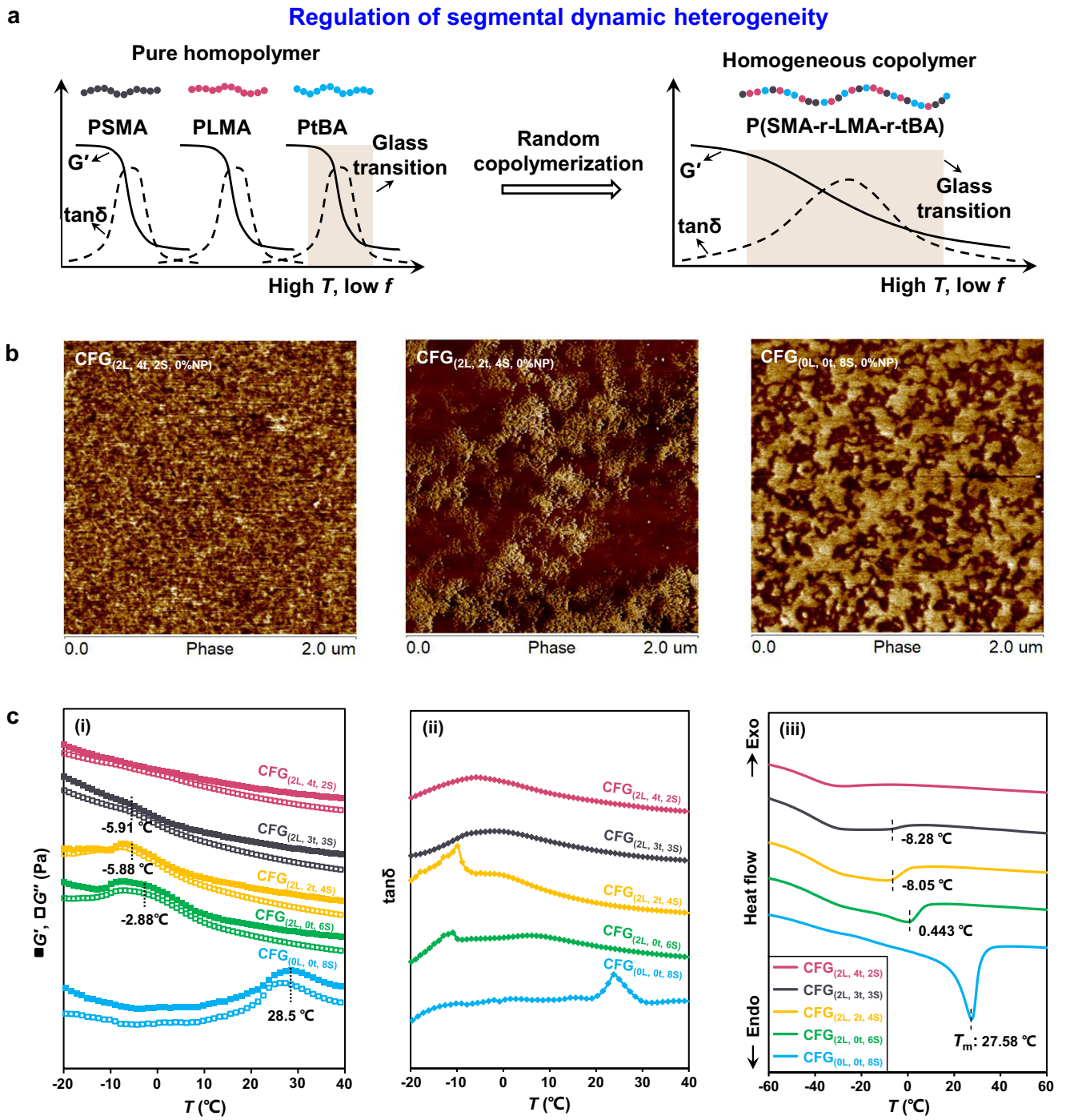

Fig. 4 | Regulation of segmental dynamic heterogeneity. a Macromolecular structure design of segmental dynamic heterogeneity for the complex-fluid-gels (CFGs) by random copolymerization to form homogeneous copolymers. **b** AFM phase images of the CFGs with varying proportions of network components. **c** Dynamic master curves (i and ii) and DSC curves (iii) for the CFGs with varying proportions of network components, respectively. PSMA poly(stearyl methacrylate), PLMA poly(lauryl methacrylate), PtBA poly(tert-butyl acrylate).

peak amplitude dissipation of vibration acceleration applied to our material is maintained at about 70% over a wide temperature range of −40 ~ 80°C (Fig. 5f and g), exhibiting stable dynamic mechanics with high energy dissipation. It can be seen that the application of our material can greatly improve the stability and reliability of electronic equipment in complex environments.

Discussion

We have developed stable dynamic mechanical polymer nanocomposites with high energy dissipation by infusing complex fluids into the nanoconfined space. The design principle is to tailor full-scale polymer dynamics across an exceptionally broad timescale by single-chain confinement. Moreover, the dynamic coupling between matrix chains and adsorbed chains on nanofiller interphase, providing an effective non-crosslinking stiffening mechanism, can enable these materials to combine high static mechanics. These materials exhibit stable G' of 10^0 ~ 10^2 MPa and high tanδ of 0.4 ~ 0.8 over the broad frequency range of 10^{-1} ~ 10^7 Hz and temperature range of -35 ~ 85°C, where the variations of tanδ and G' are extremely steady and their amplitudes are small. This work has effectively solved the inherent

https://doi.org/10.1038/s41467-024-51187-y

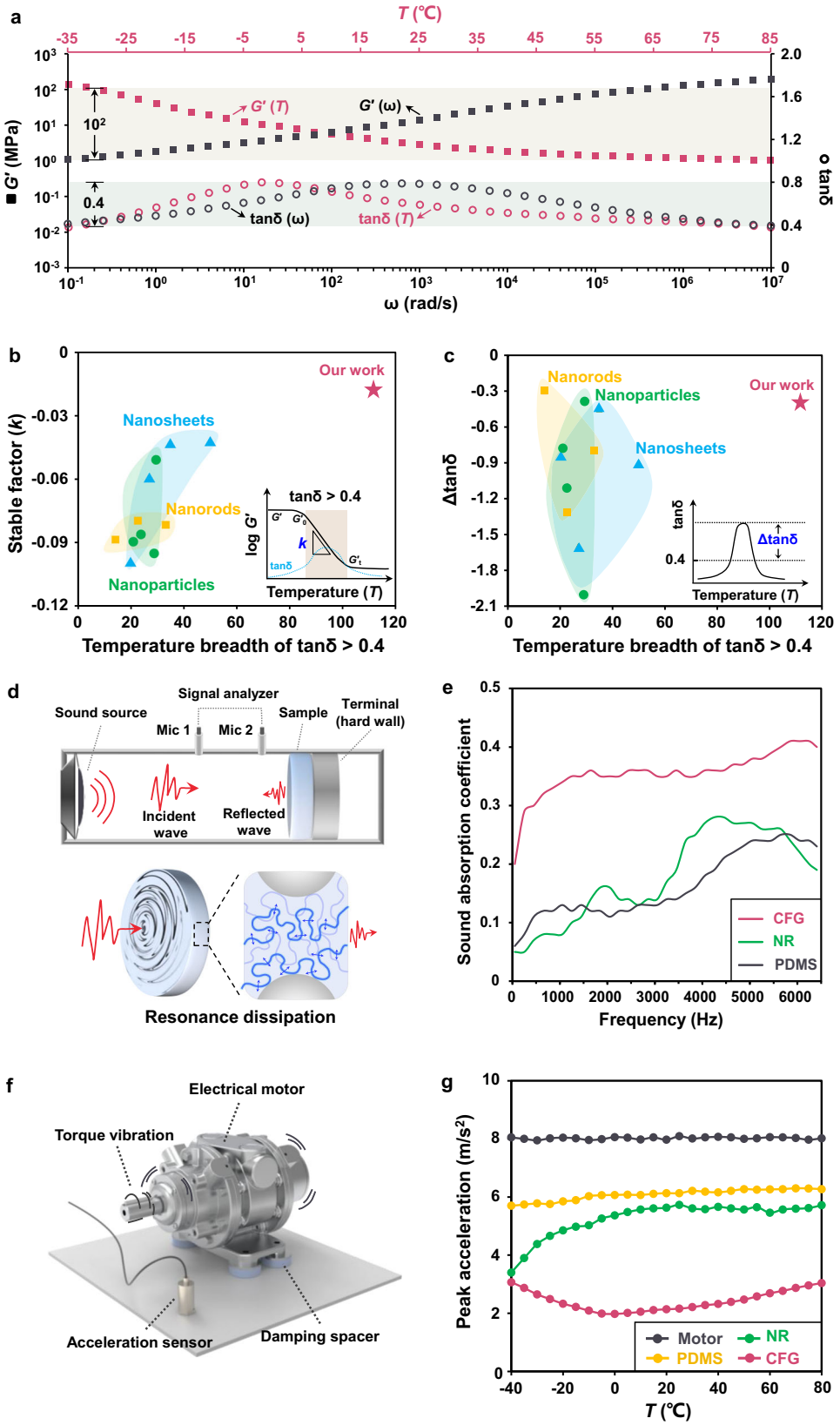

Fig. 5 | Stable dynamic mechanical CFGs with high energy dissipation. a Analysis of responsive mechanical properties of the $CFG_{(2L,\ 4t,\ 2S)}$. Dynamic master curves of storage modulus(G') (square) and loss factor (tanδ) (circle) as a function of frequency (black) and temperature (red). **b**, **c** Comparison of rate of G' change (k) and tanδ change (Δtanδ) in the temperature region of tanδ > 0.4 and temperature breadth of tanδ > 0.4 for CFGs and the reported polymer nanocomposites. $k = \log(G'_0 / G'_t) / \Delta T$, $\Delta\tan\delta = {}_0.4 - {}_t\tan\delta_{max}$. All mechanical property parameters of the reported polymer nanocomposites are listed in Supplementary Table 9. **d**, **e** Acoustic absorption experiments and sound absorption coefficient as a function of frequency in the nanocomposites. The CFG can effectively attenuate sound waves over a broad frequency range. **f**, **g** Electric motor vibration absorption demonstrative experiments of polymer nanocomposites. NR natural rubber, PDMS polydimethylsiloxane.

defects of low energy dissipation and dynamic mechanical instability of traditional polymer nanocomposites in actual applications. Therefore, we consider that this strategy can be used to develop new classes of advanced polymer nanocomposites applied in complex external environments.

Methods

Materials

Luryl methacrylate (LMA 99%, Aladdin), stearyl methacrylate (SMA 99%, Aladdin), and tert-butyl acrylate (tBA 99%, Aladdin) were all purified by the basic alumina. All other reagents (copper(I) chloride (99%), methyl alcohol, ethylene glycol dimethacrylate (EGDMA, 99%), 2,2-diethoxyacetophenone (98%), ethyl 2-bromoisobutyrate (EIBB, 98%), tris[2-(dimethylamino) ethyl] amine (Me_6TREN, 99%), and toluene) were purchased from Sigma-Aldrich and used directly. Hydrophobic silica nanoparticles were purchased from Nissan Chemical (trade name: Tol-St). Approximately 20% of the OH surface groups were replaced by short hydrocarbons, which is sufficient to render the particle hydrophobic.

Synthesis of poly(lauryl methacrylate) (PLMA) fluids

PLMA fluids were synthesized by atom transfer radical polymerization (ATRP). 50 ml toluene was added to a 100 ml flask with a stirring rod and bubbled with high purity nitrogen for 1 hour. Under nitrogen atmosphere, EIBB, CuCl, Me_6TREN, and LMA were added rapidly, and the molar ratio of EIBB / CuCl / Me_6TREN / LMA was 1:1:1:n. The polymerization was carried out at 80°C for 12 hours. After the reaction, the copper salt in the reaction solution was removed by an alumina column. PLMA fluids were slowly poured into cold methanol to precipitate, and the final product was dried under vacuum at 80°C for 24 hours.

Synthesis of complex-fluid-gels (CFGs)

The monomers (LMA, SMA, and tBA), PLMA fluid, crosslinker (ethylene glycol dimethacrylate, EGDMA), silica nanoparticles, and 0.5% photoinitiator (2,2-diethoxyacetophenone) were mixed and stirred to form uniform initial reaction mixtures. The weight ratio of crosslinker / monomer / PLMA fluid was 3:100:150 in all CFGs. The other specific feed ratios are given in Supplementary Tables 2, 3, 7 and 8. The blends were injected into the Teflon mold and photopolymerized for 2 hour under a 365 nm UV lamp at room temperature (0.1 mW / cm^2).

Molecular structural characterization

The molecular weight and distribution of polymer fluids (PLMA) were characterized by ^{1}H NMR spectra and gel permeation chromatography (GPC, Waters). ^{1}H NMR spectra were characterized in a Bruck Advanced III instrument operating at 400 MHz in $CDC1_3$. The eluent was absolute tetrahydrofuran measured at a flow rate of 1 mL/min and a column temperature of 33°C.

Rheological tests

The rheological behaviors of CFGs were characterized by the rheometer (Anton Paar model MCR-302). Frequency sweep tests were carried out at the angular frequency (ω) of 0.1 rad/s ~ 100 rad/s and shear strain (γ) of 0.3%. The frequency master curves were plotted by time-temperature superposition at the reference temperature of 25°C. The temperature sweep tests were carried out at a frequency of 10 rad/s, a shear strain of 0.3%, a temperature (T) range of -100°C ~ 200°C (2 °C/min).

Atomic force microscope

The height images and phase images were obtained by tapping mode scanning of an atomic force microscope (Bruker) using a rectangular silicon cantilever beam with a resonance frequency of 300 kHz.

X-ray scattering

Small-angle X-ray scattering (SAXS) were carried out on a SAXS system (Xeuss, Xenocs, France) equipped with a Cu-Kα source. The incident X-rays had a wavelength of 1.6 Å, and the scattering signal was recorded by a detector (Pilatus3 R 300 K, Dectris, Switzerland).

Temperature modulated differential scanning calorimetry (TMDSC)

TMDSC measurements were carried out on a Q2000 (TA Instruments), calibrated by indium and sapphire standards, using standard TZero aluminum pans. Samples were measured twice using the same procedure: ramp to 323 at 10 K/min, isothermal annealing at 323 K for 10 min to erase any thermal history, and then cooling to 173 at 10 K/min with a modulation of ± 1 K/min.

Acoustic absorption experiments

The transfer function method was performed to determine the sound absorption coefficient of materials. The acoustic probe, oscilloscope, and data acquisition were adopted to realize the prototype tests of acoustic absorber for polymer nanocomposites.

Motor vibration absorption demonstrative experiments

An electric motor was placed in an environmental chamber to test the vibration absorption of the motor by different materials at different temperatures. Vibration signals were collected by acceleration sensors.

Calculation of polymer radius of gyration (R_g) and entanglement tube diameter (a)

The polymer radius of gyration (R_g) is calculated by Eq. (1).

$$R_g = (N b^2/6)^{1/2} = (N b^2/6)^{1/2} \tag{1}$$

$$N = M_n/M_0 \tag{2}$$

where b (b = 2.53 nm) is the Kuhn length, N is the number of Kuhn monomers, M_0 (M_0 = 2513) is the molar mass of a Kuhn monomer, and M_n is the molecular weight of the polymer[30].

The diameter of the entanglement tube (a) is calculated by Eq. (3).

$$a = b N_e^{1/2} \tag{3}$$

$$N_e = M_e/M_0 \tag{4}$$

where M_e (M_e = 144k) is the entanglement molecular weight, and N_e is the number of Kuhn monomers in an entanglement strand[30].

Data availability

The data that support the findings of this study are available within the article and its Supplementary Information. All data are available from the authors upon request.

References

1. Koo, J. H. *Fundamentals, Properties, and Applications of Polymer Nanocomposites*. (Cambridge University Press, Cambridge, 2016).
2. Balazs, A. C., Emrick, T. & Russell, T. P. Nanoparticle polymer composites: where two small worlds meet. *Science* **314**, 1107–1110 (2006).
3. Ray, S. S. & Okamoto, M. Polymer/layered silicate nanocomposites: a review from preparation to processing. *Prog. Polym. Sci.* **28**, 1539–1641 (2003).
4. Baekeland, L. H. Bakelite, A new composition of matter. *Sci. Am.* **68**, 322–323 (1909).

5. Kumar, S. K., Benicewicz, B. C., Vaia, R. A. & Winey, K. I. 50th anniversary perspective: are polymer nanocomposites practical for applications? *Macromolecules* **50**, 714–731 (2017).
6. Mackay, M. E. et al. Nanoscale effects leading to non-Einstein-like decrease in viscosity. *Nat. Mater.* **2**, 762–766 (2003).
7. Senses, E., Narayanan, S., Mao, Y. & Faraone, A. Nanoscale particle motion in attractive polymer nanocomposites. *Phys. Rev. Lett.* **119**, 237801 (2017).
8. Huang, J., Zhou, J. & Liu, M. Interphase in polymer nanocomposites. *JACS Au* **2**, 280–291 (2022).
9. Capadona, J. R. et al. A versatile approach for the processing of polymer nanocomposites with self-assembled nanofibre templates. *Nat. Nanotechnol.* **2**, 765–769 (2007).
10. Chen, Y. et al. Phenolic resin-enhanced three-dimensional graphene aerogels and their epoxy nanocomposites with high mechanical and electromagnetic interference shielding performances. *Compos. Sci. Technol.* **152**, 254–262 (2017).
11. Yasmin, A., Luo, J.-J. & Daniel, I. M. Processing of expanded graphite reinforced polymer nanocomposites. *Compos. Sci. Technol.* **66**, 1182–1189 (2006).
12. Cheng, S. et al. Unexpected molecular weight effect in polymer nanocomposites. *Phys. Rev. Lett.* **116**, 038302 (2016).
13. Genix, A.-C. et al. Enhancing the mechanical properties of glassy nanocomposites by tuning polymer molecular weight. *ACS Appl. Mater. Interfaces* **10**, 33601–33610 (2018).
14. Yang, S. & Akcora, P. Deformation of chemically heterogeneous interfacial layers of polymer nanocomposites. *ACS Macro Lett.* **8**, 1635–1641 (2019).
15. You, W. & Yu, W. Slow linear viscoelastic relaxation of polymer nanocomposites: contribution from confined diffusion of nanoparticles. *Macromolecules* **52**, 9094–9104 (2019).
16. Jimenez, A. M. et al. Effects of hairy nanoparticles on polymer crystallization kinetics. *Macromolecules* **52**, 9186–9198 (2019).
17. Amini, A., Khavari, A., Barthelat, F. & Ehrlicher, A. J. Centrifugation and index matching yield a strong and transparent bioinspired nacreous composite. *Science* **373**, 1229–1234 (2021).
18. Akcora, P. et al. Anisotropic self-assembly of spherical polymer-grafted nanoparticles. *Nat. Mater.* **8**, 354–359 (2009).
19. Akcora, P. et al. "Gel-like" mechanical reinforcement in polymer nanocomposite melts. *Macromolecules* **43**, 1003–1010 (2010).
20. Maillard, D. et al. Mechanical properties of thin glassy polymer films filled with spherical polymer-grafted nanoparticles. *Nano lett.* **12**, 3909–3914 (2012).
21. Rittigstein, P., Priestley, R. D., Broadbelt, L. J. & Torkelson, J. M. Model polymer nanocomposites provide an understanding of confinement effects in real nanocomposites. *Nat. Mater.* **6**, 278–282 (2007).
22. Bailey, E. J. & Winey, K. I. Dynamics of polymer segments, polymer chains, and nanoparticles in polymer nanocomposite melts: a review. *Prog. Polym. Sci.* **105**, 101242 (2020).
23. Shaw, M. T. & Macknight, W. J. *Introduction to Polymer Viscoelasticity* Subsequent edn, Vol. 320 (Wiley–Blackwell, 1983).
24. Tracht, U. et al. Length scale of dynamic heterogeneities at the glass transition determined by multidimensional nuclear magnetic resonance. *Phys. Rev. Lett.* **81**, 2727–2730 (1998).
25. Russell, E. V. & Israeloff, N. Direct observation of molecular cooperativity near the glass transition. *Nature* **408**, 695–698 (2000).
26. Richter, D. & Kruteva, M. Polymer dynamics under confinement. *Soft Matter* **15**, 7316–7349 (2019).
27. Gin, P. et al. Revealed architectures of adsorbed polymer chains at solid-polymer melt interfaces. *Phys. Rev. Lett.* **109**, 265501 (2012).
28. Tang, S., Wang, M. & Olsen, B. D. Anomalous self-diffusion and sticky rouse dynamics in associative protein hydrogels. *J. Am. Chem. Soc.* **137**, 3946–3957 (2015).
29. Brandrup, J., Immergut, E. H. & Grulke, E. A. *Polymer Handbook*. 4th edn, Vol. 2336 (Wiley–Blackwel, 1999).
30. Mark, J. E. *Physical Properties of Polymers Handbook* 2nd edn, Vol. 1076 (Springer New York, 2007).
31. Chen, Q. et al. Mechanical reinforcement of polymer nanocomposites from percolation of a nanoparticle network. *ACS Macro Lett.* **4**, 398–402 (2015).
32. Guinier, A., Fournet, G. & Yudowitch, K. L. *Small-Angle Scattering of X-rays*. (Wiley, New York,1955).
33. Schaefer, D. W. Polymers, fractals, and ceramic materials. *Science* **243**, 1023–1027 (1989).
34. Holt, A. P. et al. Dynamics at the polymer/nanoparticle interface in poly(2-vinylpyridine)/silica nanocomposites. *Macromolecules* **47**, 1837–1843 (2014).
35. Klonos, P. et al. Morphology and molecular dynamics investigation of PDMS adsorbed on titania nanoparticles: effects of polymer molecular weight. *Eur. Polym. J.* **74**, 64–80 (2016).

Acknowledgements

This research was supported by the National Natural Science Foundation of China (22341301, M. L.), the National Key Research and Development Project (2022YFA503000, M. L.), the National Natural Science Foundation of China (22175010, M. L.), and the China Postdoctoral Science Foundation (2021M700317, J. H.).

Author contributions

M. L. contributed to the initiating idea and J. H. performed all experiments. M. L., T. Z., and J. Z. contributed to the analysis of mechanical properties and the theoretical analysis of the relaxation of polymer chains. H. Z., Longhao Z., W. S., Y. Y., and Li Z. designed the rheological behavior of complex-fluid-gels. The paper was written by J. H., and M. L., and edited by all the authors. All the authors analyzed the data of experiments.

Competing interests

The authors declare no competing interests.

Additional information

Supplementary information The online version contains supplementary material available at https://doi.org/10.1038/s41467-024-51187-y.

Correspondence and requests for materials should be addressed to Mingjie Liu.

Peer review information *Nature Communications* thanks Humberto Almeida, Davide De Focatiis and the other, anonymous, reviewer(s) for their contribution to the peer review of this work. A peer review file is available.

Supplementary Information

Full-scale polymer relaxation induced by single-chain confinement enhances mechanical stability of nanocomposites

Jin Huang, Hangsheng Zhou, Longhao Zhang, Li Zhang, Wei Shi, Yingchao Yang, Jiajia Zhou, Tianyi Zhao, Mingjie Liu*
Correspondence to: liumj@buaa.edu.cn

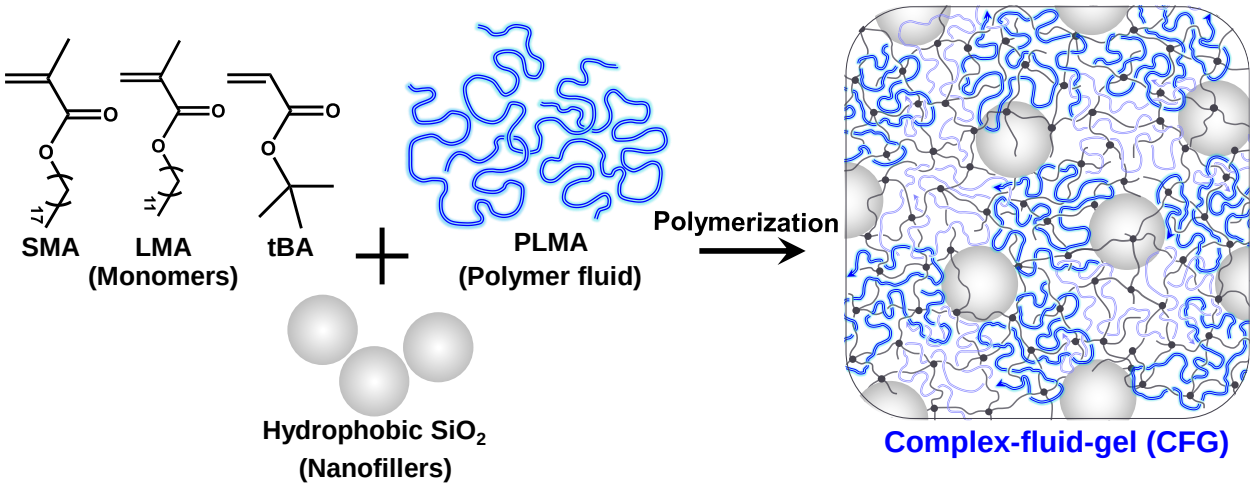

Supplementary Figure 1. Synthesis of complex-fluid gels (CFGs).

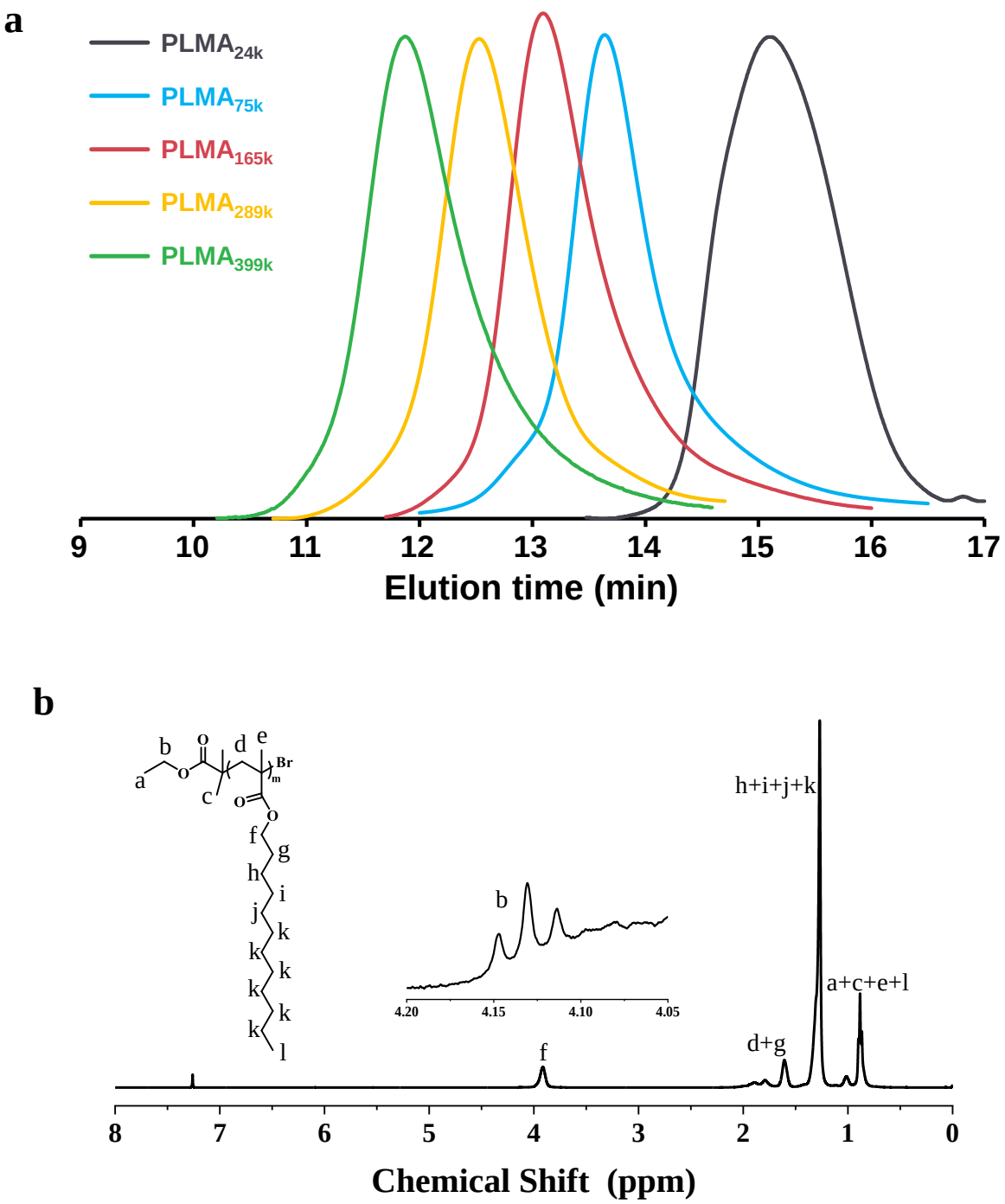

Supplementary Figure 2. Molecular structural characterization. **(a)** GPC traces of poly(lauryl methacrylate) (PLMA) fluids. **(b)** ^{1}H-NMR spectra of $PLMA_{24k}$ fluid.

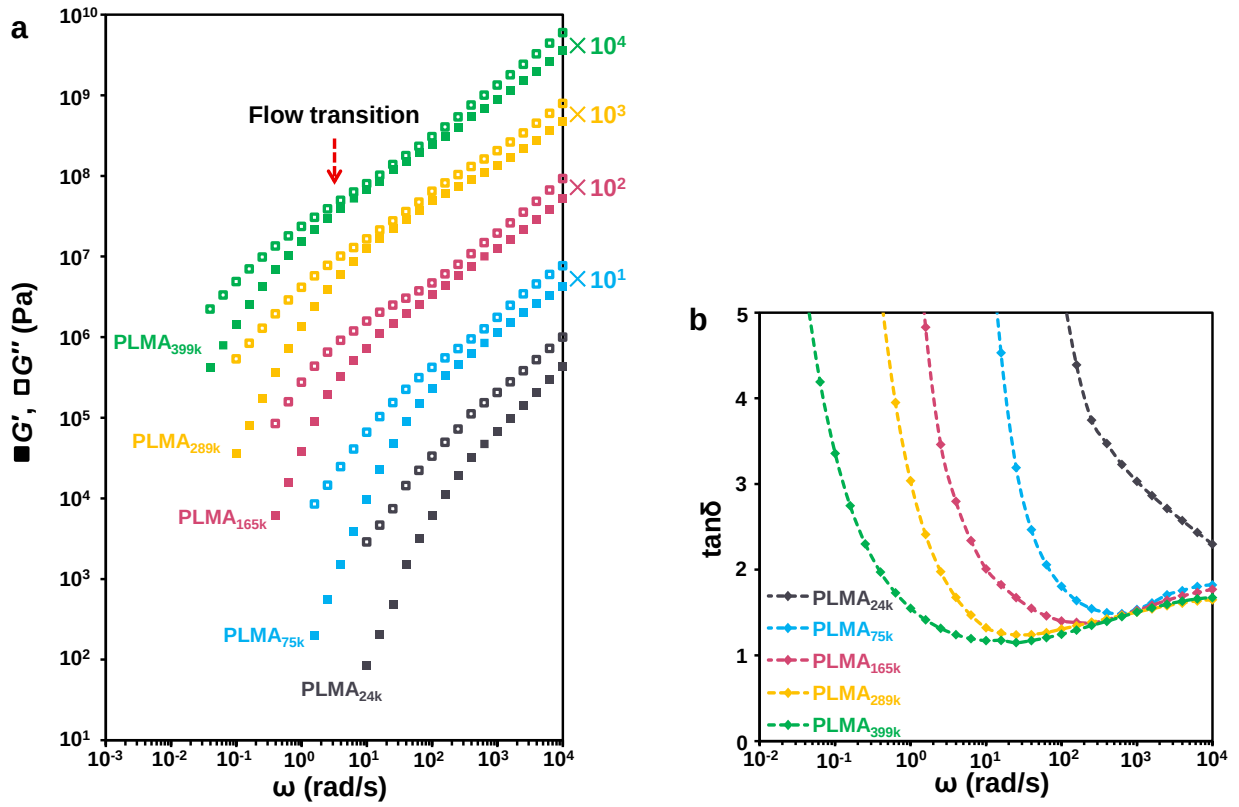

Supplementary Figure 3. Dynamic mechanical behavior of PLMA fluids. **(a)** Vertically shifted master curves of storage modulus (*G′*, filled squares) and loss modulus (*G″*, open squares) for PLMA fluids with varying molecular weight as a function of frequency at 25℃. **(b)** Frequency dependence of master curves of loss factor (tanδ) for PLMA fluids with varying molecular weight at 25℃.

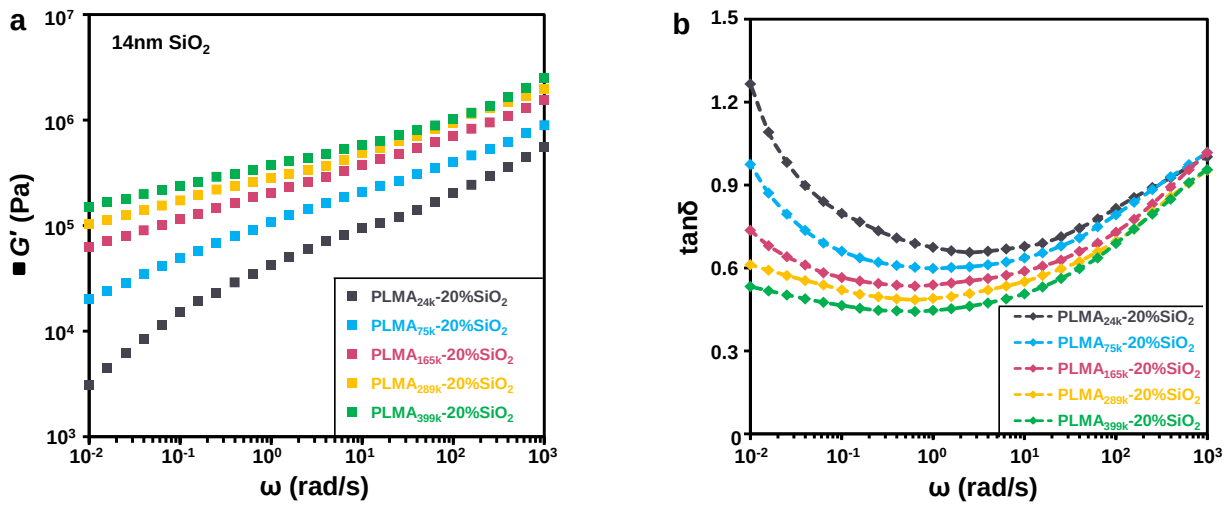

Supplementary Figure 4. Dynamic mechanical behavior of nanocomposite PLMA fluids. Frequency dependence of master curves of **(a)** storage modulus (G') and **(b)** loss factor (tanδ) for PLMA fluids with $\Phi_{\text{NP-14nm}} = 20\%$ and varying $M_{\text{n (PLMA fluid)}}$. $M_{\text{n (PLMA fluid)}}$: molecular weight of PLMA fluids, $\Phi_{\text{NP-14nm}}$: weight fraction of nanoparticle.

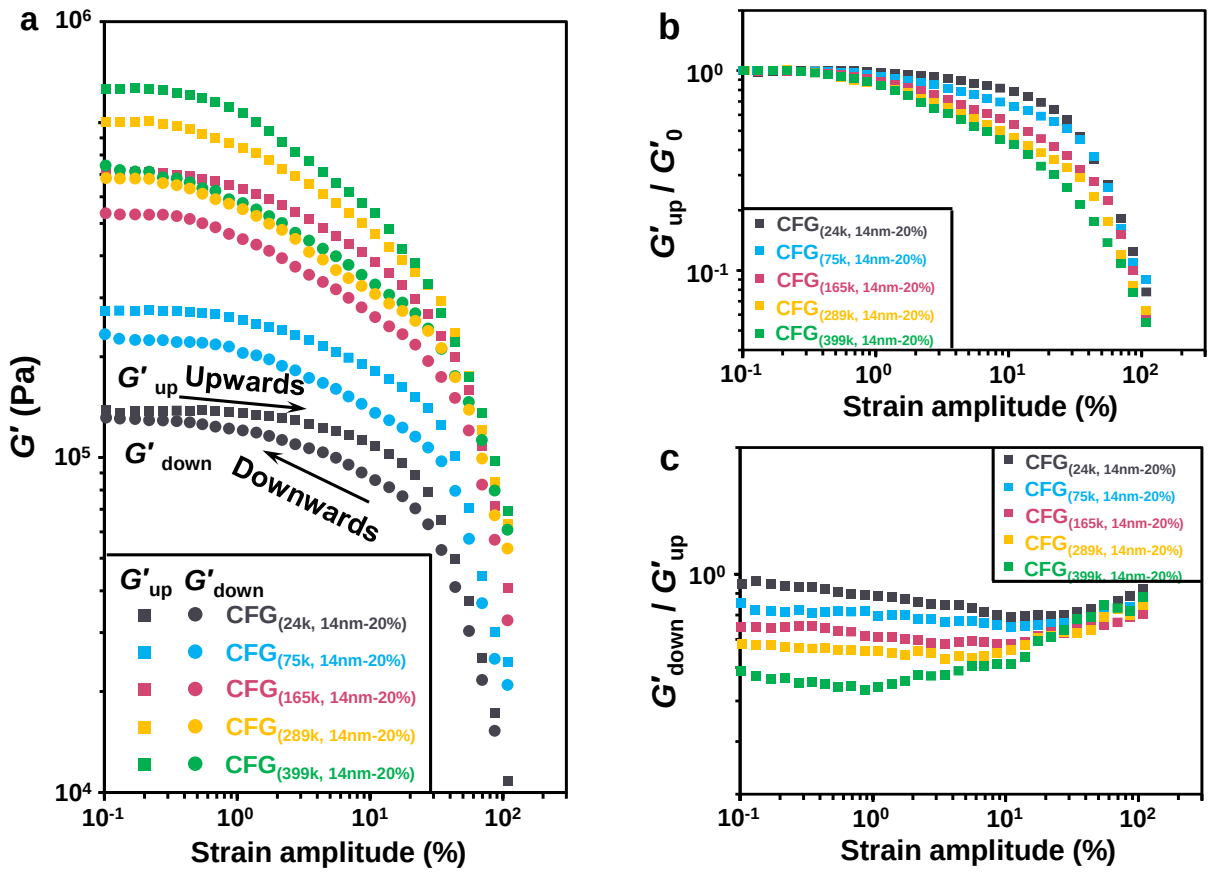

Supplementary Figure 5. Amplitude sweeps for CFGs with different chain length. **(a)** Storage modulus of upward amplitude sweep (G'_{up}) and storage modulus of backward amplitude sweep (G'_{down}) for CFGs with $\Phi_{NP\text{-}14nm}$ = 20% and varying $M_{n\ (PLMA\ fluid)}$ as a function of the strain amplitude at the frequency of 1 rad/s and temperature of 25°C. **(b)** G'_{up} / G'_0 and **(c)** G'_{up} / G'_{down} for CFGs with $\Phi_{NP\text{-}14nm}$ = 20% and varying $M_{n\ (PLMA\ fluid)}$ as a function of the strain amplitude. $M_{n\ (PLMA\ fluid)}$: molecular weight of PLMA fluids, $\Phi_{NP\text{-}14nm}$: weight fraction of nanoparticle, G'_0: original storage modulus.

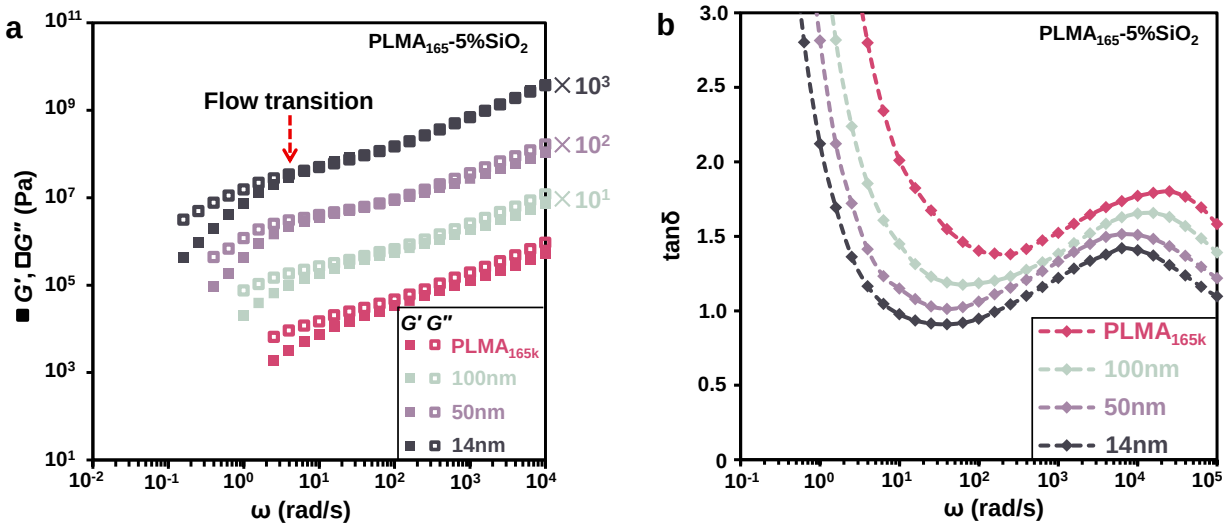

Supplementary Figure 6. Dynamic mechanical behavior of nanocomposite PLMA fluids with varying particle sizes. Frequency dependence of master curves of **(a)** storage modulus (G') and **(b)** loss factor (tanδ) for PLMA fluids with $\Phi_{nanoparticle}$ = 5% and varying particle sizes. $\Phi_{nanoparticle}$: weight fraction of nanoparticle.

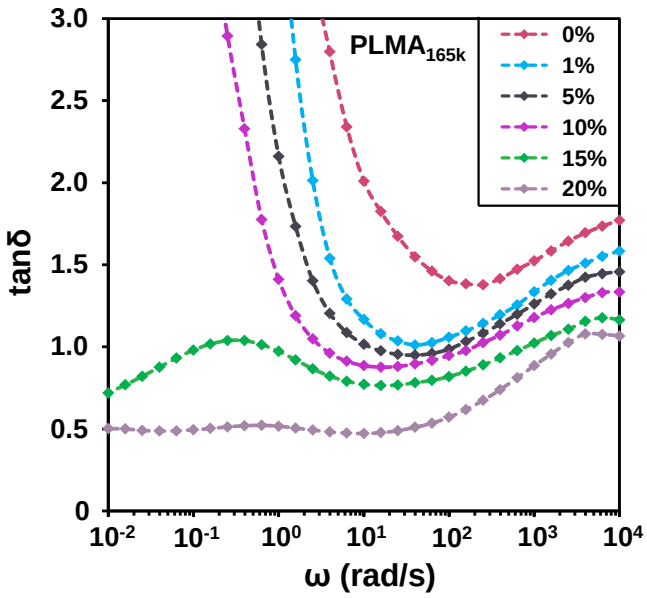

Supplementary Figure 7. Frequency dependence of loss factor (tanδ) of $PLMA_{165k}$ fluids with increasing weight fraction of 14 nm nanoparticles.

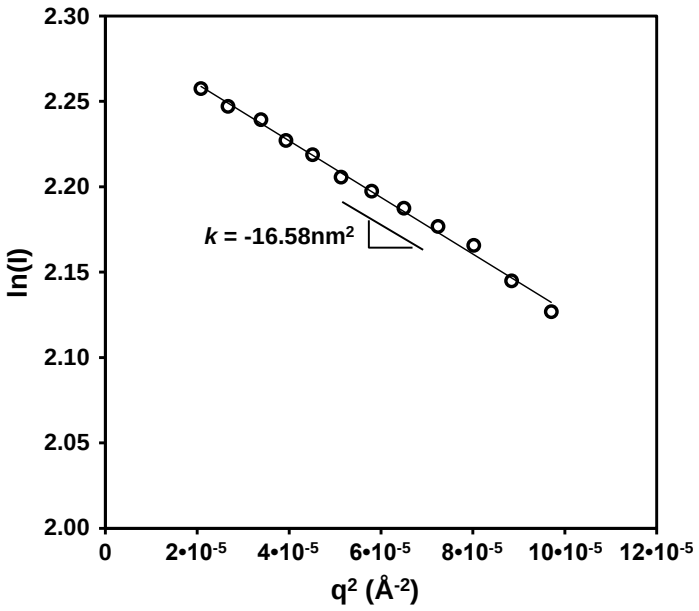

Supplementary Figure 8. ln(I) as a function of q^2 for the CFG with low nanoparticle loading ($\Phi_{14nm\text{-}NP}$ = 1%).

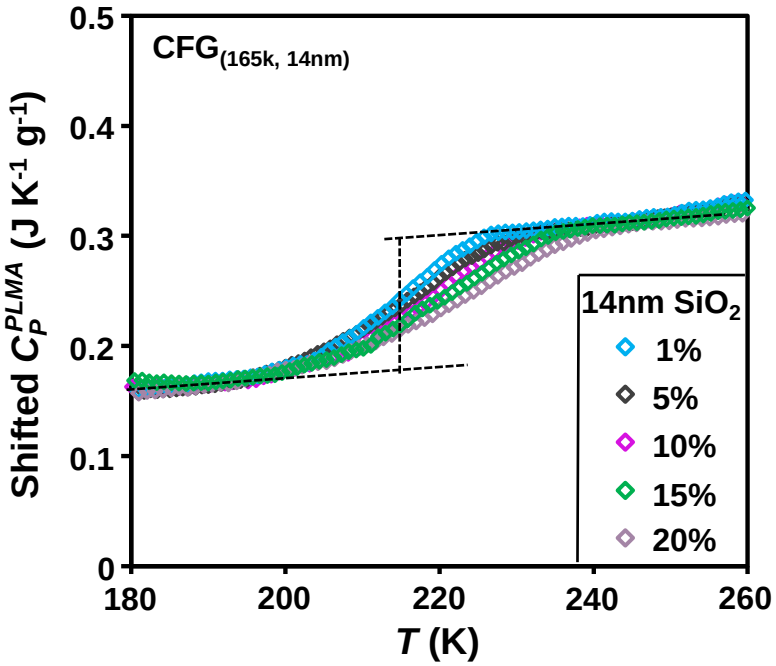

Supplementary Figure 9. Specific heat capacity of the polymer fraction in the nanocomposites with different SiO_2 loading. The curves are arbitrarily shifted to align to illustrate the broadening of the glass transition step.

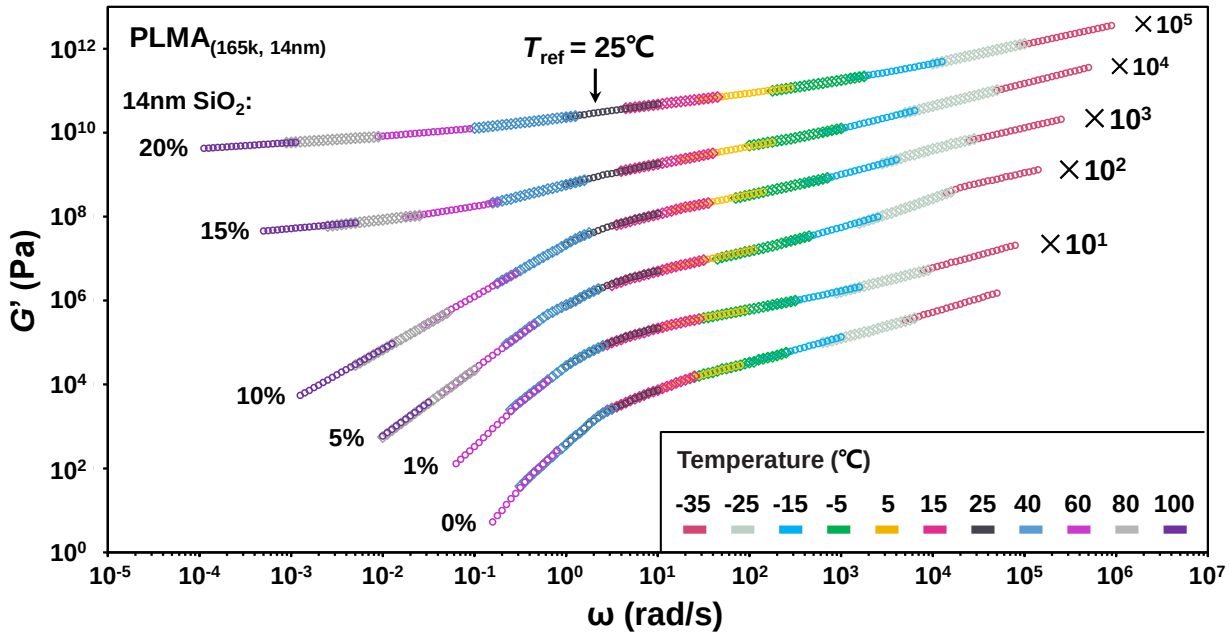

Supplementary Figure 10. Master curves of PLMA with different filler content drawn by the time-temperature superposition principle with T_{ref} = 25°C.

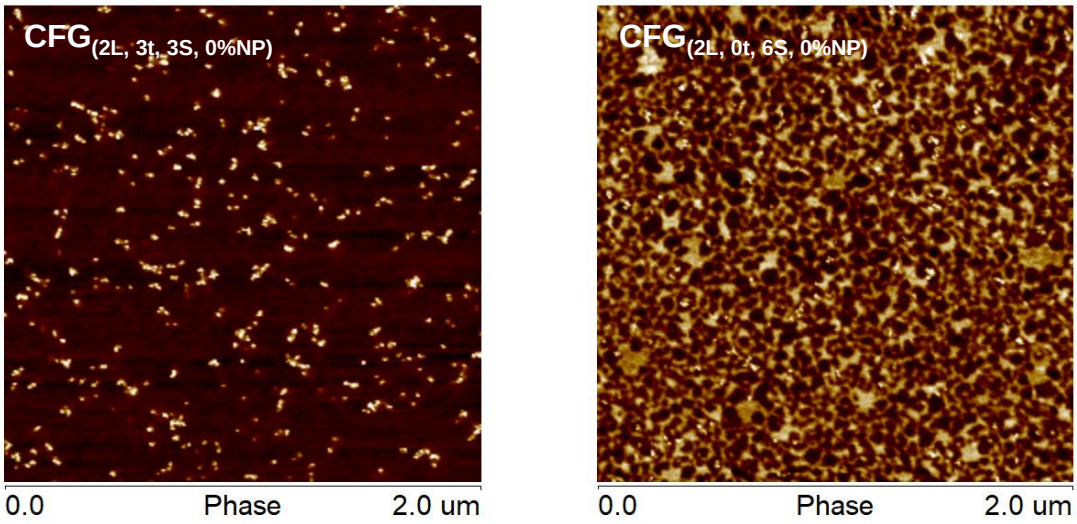

Supplementary Figure 11. AFM phase images of the CFGs with varying proportion of network components.

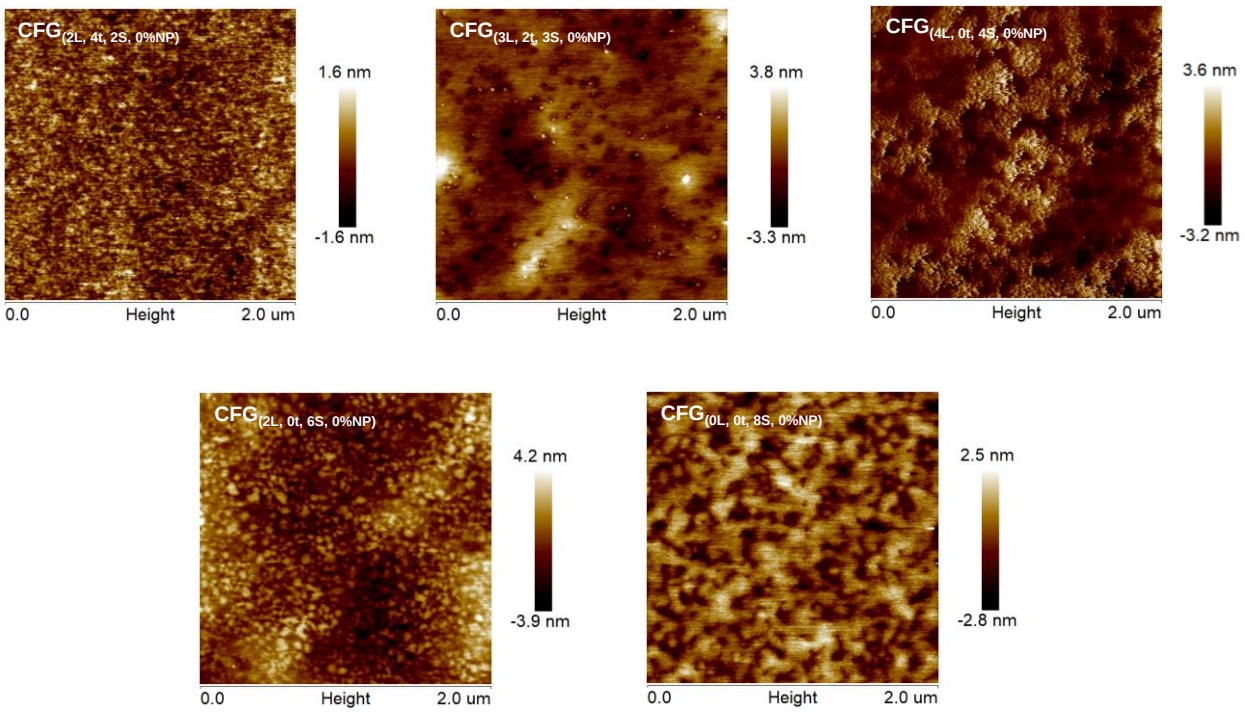

Supplementary Figure 12. AFM height images of the CFGs with varying proportion of network components.

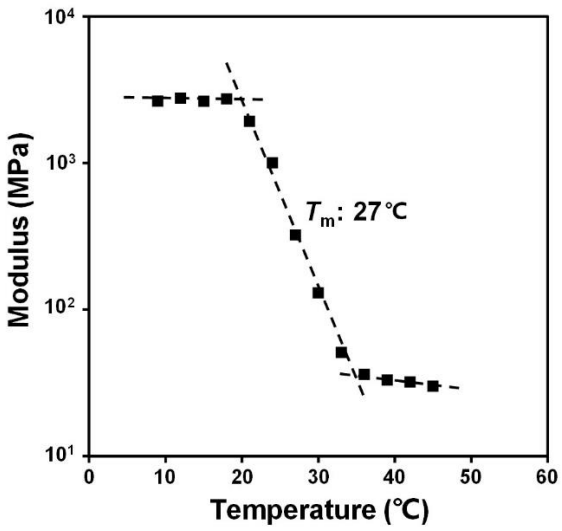

Supplementary Figure 13. Modulus versus temperature of bright domain in the CFGs with crystalline component (PSMA).

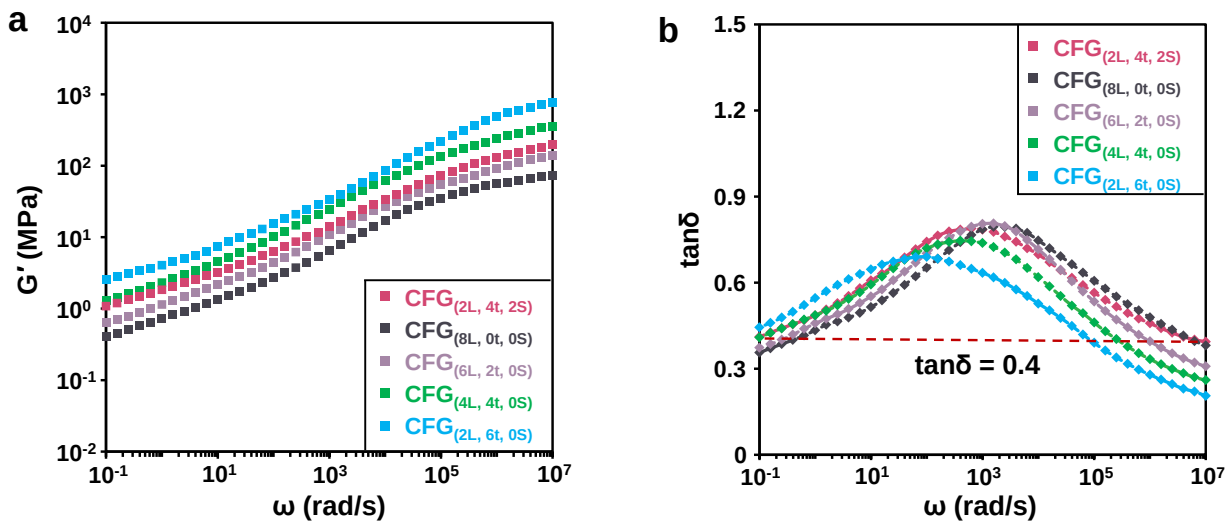

Supplementary Figure 14. Dynamic mechanical behavior of CFGs with multiple components. Frequency dependence of master curves of **(a)** storage modulus (*G′*) and **(b)** loss factor (tanδ) for CFGs with multiple components.

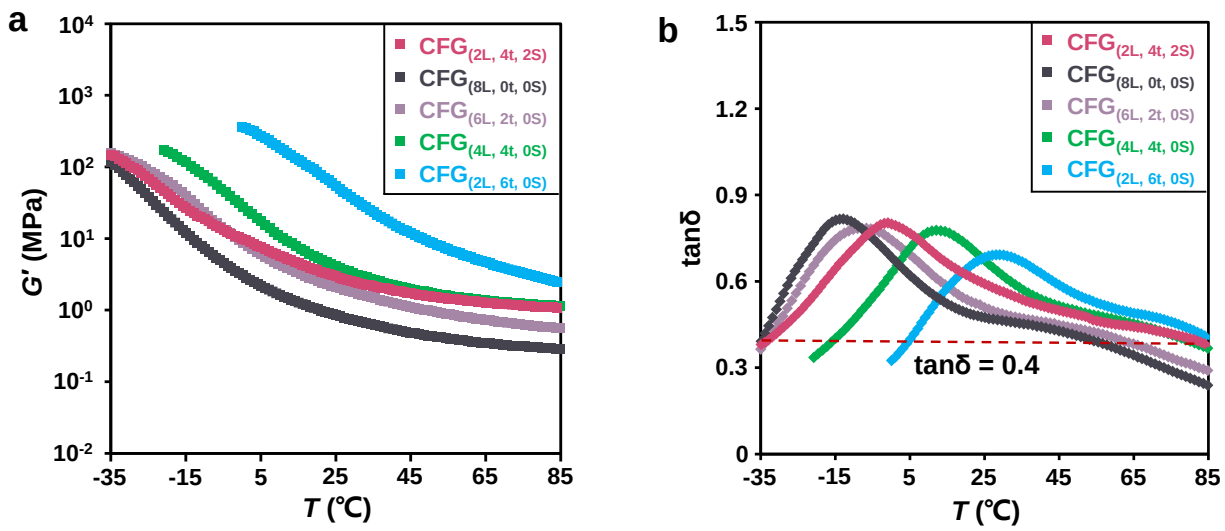

Supplementary Figure 15. Dynamic mechanical behavior of CFGs with multiple components. Temperature dependence of master curves of **(a)** storage modulus (*G′*) and **(b)** loss factor (tanδ) for CFGs with multiple components.

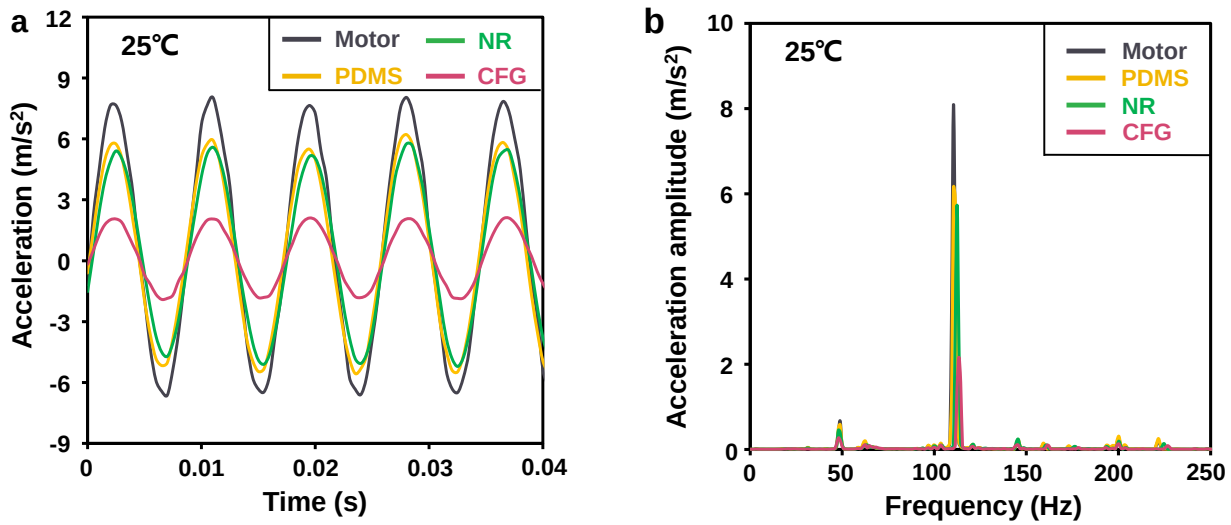

Supplementary Figure 16. Electric motor vibration absorption demonstrative experiments. **(a)** Vibration acceleration on different elastomers as a function of time at 25℃. **(b)** Acceleration amplitude on different elastomers as a function of frequency at 25℃. NR: natural rubber, PDMS: polydimethylsiloxane.

Supplementary Table 1. Molecular characteristics of PLMA fluids.

PLMA fluids	DP	M_n (kg/mol)	M_w (kg/mol)	PDI
$PLMA_{100}$	95	24.2	31.4	1.31
$PLMA_{300}$	296	75.3	91.9	1.22
$PLMA_{600}$	649	165.1	208.0	1.26
$PLMA_{1000}$	1019	258.8	313.2	1.21
$PLMA_{1500}$	1569	398.5	490.2	1.23

Supplementary Table 2. Molecular characteristics of CFGs with various molecular weight of PLMA fluids.

Samples [a]	$M_{n\ (PLMA\ fluid)}$ [b] (kg/mol)	$\Phi_{NP\text{-}14nm}$ [c] (%)
CFG$_{(24k,\ 14nm\text{-}20\%)}$	24	20
CFG$_{(75k,\ 14nm\text{-}20\%)}$	75	20
CFG$_{(165k,\ 14nm\text{-}20\%)}$	165	20
CFG$_{(289k,\ 14nm\text{-}20\%)}$	289	20
CFG$_{(399k,\ 14nm\text{-}20\%)}$	399	20
CFG$_{(14nm\text{-}20\%)}$	0	20

[a] The weight ratio of crosslinker / PLMA monomer / PLMA fluid is 3:100:150 in all CFGs.

[b] Molecular weight of PLMA fluid. [c] Weight fraction of 14 nm nanoparticles.

Supplementary Table 3. Molecular characteristics of CFGs with various nanoparticle size.

Samples [a]	$M_{n\ (PLMA\ fluid)}$ [b] (kg/mol)	Φ_{NP} [c] (%)	NP size (nm)
CFG$_{(165k,\ 14nm\text{-}5\%)}$	165	5	14
CFG$_{(165k,\ 50nm\text{-}5\%)}$	165	5	50
CFG$_{(165k,\ 100nm\text{-}5\%)}$	165	5	100
CFG$_{(165k)}$	165	0	

[a] The weight ratio of crosslinker / PLMA monomer / PLMA fluid is 3:100:150 in all CFGs.

[b] Molecular weight of PLMA fluid. [c] Weight fraction of 14 nm nanoparticles.

Supplementary Table 4. Surface-to-surface distance (d_{ss}) and the confinement parameter of CFGs with varying content of 14 nm nanoparticles.

NP% Mass (volume)	Surface-to-surface distance (d_{ss}) (nm)	$d_{ss} / 2R_g$ [a]	d_{ss} / a [b]
1 (0.5)	56.4	3.36	2.95
5 (2.5)	27.2	1.62	1.42
10 (5.0)	18.7	1.12	0.98
15 (7.5)	14.6	0.87	0.76
20 (10.0)	11.9	0.71	0.62

[a] Polymer radius of gyration. [b] Entanglement tube diameter.

Supplementary Table 5. Shift factors of PLMA fluids with various weight fraction of 14 nm nanoparticles.

Temperature (°C)	Log($a_{PLMA\text{-}0\%SiO_2}$)	Log($a_{PLMA\text{-}0\%SiO_2}$)	Log($a_{PLMA\text{-}0\%SiO_2}$)	Log($a_{PLMA\text{-}0\%SiO_2}$)	Log($a_{PLMA\text{-}0\%SiO_2}$)	Log($a_{PLMA\text{-}0\%SiO_2}$)
-35	3.67	3.9	4.15	4.4	4.7	4.95
-25	2.8	2.95	3.2	3.45	3.7	4
-15	2	2.2	2.4	2.6	2.8	3.1
-5	1.4	1.5	1.65	1.85	2	2.25
5	0.9	0.95	1.05	1.15	1.25	1.45
15	0.4	0.45	0.5	0.55	0.6	0.65
25	0	0	0	0	0	0
40	-0.5	-0.6	-0.65	-0.75	-0.8	-0.9
60	-1.1	-1.2	-1.35	-1.55	-1.75	-2.05
80			-2	-2.3	-2.6	-3.05
100			-2.5	-2.9	-3.3	-3.95

Supplementary Table 6. Williams–Landel–Ferry (WLF) equation parameters of PLMA fluids with various weight fraction of 14 nm nanoparticles.

Sample	$\Phi_{\text{NP-14nm}}$ [a]	C_1	C_2
$\text{PLMA}_{(165k,\ 14nm\text{-}0\%)}$	0%	6.31	162.32
$\text{PLMA}_{(165k,\ 14nm\text{-}1\%)}$	1%	6.95	167.54
$\text{PLMA}_{(165k,\ 14nm\text{-}5\%)}$	5%	8.76	186.96
$\text{PLMA}_{(165k,\ 14nm\text{-}10\%)}$	10%	10.92	209.1
$\text{PLMA}_{(165k,\ 14nm\text{-}15\%)}$	15%	13.41	231.22
$\text{PLMA}_{(165k,\ 14nm\text{-}20\%)}$	20%	19.35	294.52

[a] Weight fraction of 14 nm nanoparticles.

Supplementary Table 7. Molecular characteristics of CFGs with varying proportion of network components.

CFGs [a]	$\Phi_{\text{NP-14nm}}$ [b] (%)	$M_{\text{n (PLMA fluid)}}$ [c] (kg/mol)	$\Phi_{\text{(Network)}}$ [d] (%)
			PLMA, PtBA, PSMA
$CFG_{(2L,\ 4t,\ 2S,\ 0\%NP)}$	0	165	10, 20, 10
$CFG_{(2L,\ 3t,\ 3S,\ 0\%NP)}$	0	165	10, 15, 15
$CFG_{(2L,\ 2t,\ 4S,\ 0\%NP)}$	0	165	10, 10, 20
$CFG_{(2L,\ 0t,\ 6S,\ 0\%NP)}$	0	165	10, 0, 30
$CFG_{(0L,\ 0t,\ 8S,\ 0\%NP)}$	0	165	0, 0, 40
$CFG_{(2L,\ 4t,\ 2S)}$	20	165	7.5, 15, 7.5
$CFG_{(2L,\ 3t,\ 3S)}$	20	165	8, 11, 11
$CFG_{(2L,\ 2t,\ 4S)}$	20	165	7.5, 7.5, 15
$CFG_{(2L,\ 0t,\ 6S)}$	20	165	7.5, 0, 22.5
$CFG_{(0L,\ 0t,\ 8S)}$	20	165	0, 0, 30

[a] The weight ratio of crosslinker / PLMA monomer / PLMA fluid is 3:100:150 in all CFGs.

[b] Weight fraction of 14 nm nanoparticles. [c] Molecular weight of PLMA fluid. [d] Weight fraction of PLMA network.

Supplementary Table 8. Molecular characteristics of CFGs with varying content of crystalline component.

CFGs [a]	$\Phi_{NP\text{-}14nm}$ [b] (%)	$\Phi_{(Network)}$ [c] (%)
		PLMA, PtBA, PSMA
$CFG_{(2L,\ 4t,\ 2S)}$	20	7.5, 15, 7.5
$CFG_{(8L,\ 0t,\ 0S)}$	20	30, 0, 0
$CFG_{(6L,\ 2t,\ 0S)}$	20	22.5, 7.5, 0
$CFG_{(4L,\ 4t,\ 0S)}$	20	15, 15, 0
$CFG_{(2L,\ 6t,\ 0S)}$	20	7.5, 22.5, 0

[a] The weight ratio of crosslinker / monomer / PLMA fluid is 3:100:150 in all CFGs.

[b] Weight fraction of 14 nm nanoparticles. [c] Weight fraction of network components.

Supplementary Table 9. Mechanical property parameters of the reported damping materials.

Nanofillers	Polymer nanocomposites	tanδ > 0.4 (°C width)	Δtanδ [a]	*k* [b]	Ref.
Nanoparticles	Nitrile butadiene rubber	28.4	-2	-0.095	(*1*)
	Poly(ether imide) / PMMA	23	-1.1	-0.087	(*2*)
	Polyurethane	30.4	-0.38	-0.0515	(*3*)
	Epoxy resin	21	-0.78	-0.0893	(*4*)
Nanorods	Epoxy resin	33	-0.8	-0.0818	(*5*)
	Polycarbonate	22.5	-1.32	-0.08	(*6*)
	Epoxy resin	14	-0.3	0.0888	(*7*)
Nanosheets	Polyurethane	35	-0.45	-0.0434	(*8*)
	Fluoroelastomer	50	-0.9	-0.0425	(*9*)
	Natural rubber	27	-1.6	-0.0593	(*10*)
	Epoxy resin	20	-0.85	-0.1	(*11*)

[a] Tanδ change in the temperature region of tanδ > 0.4, $\Delta\tan\delta = 0.4 - \tan\delta_{max}$. [b] G' change rate (k) in the temperature region of tanδ > 0.4, $k = \log G' / T$.

References

1. Zhao, X. Y. *et al.* Nitrile butadiene rubber/hindered phenol nanocomposites with improved strength and high damping performance. *Polymer* **48**, 6056-6063 (2007).
2. Comer, A., Heilman, A. & Kalika, D. Dynamic relaxation characteristics of polymer nanocomposites based on poly (ether imide) and poly (methyl methacrylate). *Polymer* **51**, 5245-5254 (2010).
3. Praveen, S. *et al.* Tunable viscoelastic and vibration damping properties of a segmented polyurethane synergistically reinforced with carbon black and anisotropic additives. *Appl. Acoust.* **170**, 107535 (2020).
4. Zhang, X. *et al.* Strengthened magnetic epoxy nanocomposites with protruding nanoparticles on the graphene nanosheets. *Polymer* **54**, 3594-3604 (2013).
5. Jagtap, S. B. & Ratna, D. Novel method of dispersion of multiwalled carbon nanotubes in a flexible epoxy matrix. *J. Appl. Polym. Sci.* **130**, 2610-2618 (2013).
6. Gong, Z., Gong, J., Yan, X., Gao, S. & Wang, B. Investigation of the effects of temperature and strain on the damping properties of polycarbonate/multiwalled carbon nanotube composites. *J. Phys. Chem. C* **115**, 18468-18472 (2011).
7. Zeng, S., Reyes, C., Liu, J., Rodgers, P. & Sun, A. L. Facile hydroxylation of halloysite nanotubes for epoxy nanocomposite applications. *Polymer* **55**, 6519-6528 (2014).
8. Dehghan, P. *et al.* Synthesis and design of polyurethane and its nanocomposites derived from canola‐castor oil: Mechanical, thermal and shape memory properties. *J. Polym. Sci.* **58**, 3082-3094 (2020).
9. Gao, W. & Guo, J. A novel processing method namely fast evaporation mixing to prepare fluoroelastomer/montmorillonite composites. *Compos. Sci. Technol.* **139**, 26-35 (2017).
10. Wang, Y., Zhang, H., Wu, Y., Yang, J. & Zhang, L. Preparation and properties of natural rubber/rectorite nanocomposites. *Eur. Polym. J.* **41**, 2776-2783 (2005).
11. Song, S. *et al.* Enhanced thermal conductivity of epoxy-graphene composites by using non-oxidized graphene flakes with non-covalent functionalization. *Adv. Mater.* **25**, 732-737 (2013).